Please cite as: González-Pino, I., Pérez-Iribarren, E., Campos-Celador, A., Terés-Zubiaga, J., Las-Heras-Casas, J.. Modelling and experimental characterization of a Stirling engine-based domestic micro-CHP device. Energy Conversion and Management, 2020, 225, 113429

ENERGY CONVERSION AND MANAGEMENT
https://doi.org/10.1016/j.enconman.2020.113429

Modelling and experimental characterization of a Stirling engine-based domestic micro-CHP device

González-Pino I.[a*], Pérez-Iribarren E.[a],Campos-Celador A.[b], Terés-Zubiaga J.[a], Las-Heras-Casas J.[c]

[a] ENEDI Research Group, Department of Energy Engineering, Faculty of Engineering of Bilbao, University of the Basque Country UPV/EHU, Plaza Torres Quevedo 1, Bilbao 48013, Spain.

[b] ENEDI Research Group, Department of Energy Engineering, Faculty of Engineering of Gipuzkoa, University of the Basque Country UPV/EHU, Avenida. Otaola 29, Eibar 20600, Spain.

[c]TENECO Research Group, Area of Thermal Engineering of the Department of Mechanical Engineering, University of La Rioja, Luis de Ulloa 20, Logroño 26004, Spain.

[*] Corresponding author. Tel.: +34946017364. Fax: +34946017800. E-mail: iker.gonzalezp@ehu.eus

ABSTRACT

This article presents and validates a dynamic model of a natural gas-run micro-CHP boiler, whose primary mover is a Stirling engine. From a preliminary literature review on the modelling of this kind of devices, and taking into consideration the goal of performing full system simulations, a semi-empirical one is proposed. Specifically, the model consists of the direct application of general mass and energy conservation principles, supported by empirical expressions based on parametric factors that must be determined experimentally. For that purpose, an experimental test-rig was developed, and a full characterization of a Stirling unit was carried out in order to calibrate the model. Unlike other previous models, the one developed throughout this article fully takes into account both the dynamics that occur during the start-up and cool-down periods, as well as the partial load performance of the engine, providing high precision results while maintaining the simplicity required in energy simulation environments. Calculations during the validation phase show that, when operating at normal conditions, the model is able to reproduce the electricity output and the water delivery temperature with errors below 2.4% and 0.9% in any case, respectively; while during a full-length test, the mean errors for the energy exchanges due to fuel input, thermal output and electrical output were 1.4%, 0.4% and 0.1%, respectively.

Keywords: *micro-CHP*, *Stirling engine, dynamic model, part-load, experimental characterization, validation*

Nomenclature

Adj-R^2	Adjusted coefficient of determination
amb	Relative to indoor ambient conditions
comb	Relative to the combustion

c	Specific heat
E	Electricity (the "·" above indicates power)
F	Fuel energy (the "·" above indicates power)
H	Enthalpy (the "·" above indicates power)
m	Mass (the "·" above indicates flow)
MC	Thermal mass
p-value	Probability
Q	Heat (the "·" above indicates power)
T	Temperature
UA	Effective heat transfer coefficient

Abbreviations

AB	Auxiliary burner
BES	Building energy simulation
CHP	Cogeneration
CVRMSE	Normalized root mean square error
DHW	Domestic hot water
ECU	Electronic control unit
EU	European Union
LCCE	Laboratory for the Quality Control in Buildings
LHV	Lower heating value
NMBE	Normalized mean bias error
PLC	Programmable logic controller
SE	Stirling engine
μCHP	Micro-cogeneration

Greek symbols

α	Part-load ratio
η	Energy efficiency

Subscripts

ab	Relative to the auxiliary burner
air	Oxidizing air
cond	Relative to condensing water vapour
cw	Relative to the cooling water
cw,i	Relative to the inlet cooling water
cw,o	Relative to the outlet cooling water
e	Relative to electricity
eng	Relative to the engine-block
exh	Relative to the exhaust gases
f	Relative to fuel
gross	Relative to gross output
head	Relative to the head of the engine
HX	Relative to the heat exchanger
loss	Relative to heat losses
net	Relative to net output
nom	Relative to nominal conditions
ref	Relative to reference values
se	Relative to the Stirling engine
shut-down	Relative to shut-down process
standby	Relative to standby-mode
t	Relative to heat

Superscripts

°	Relative to normal conditions
ab	Relative to the auxiliary burner
e	Relative to electricity
f	Relative to fuel
lim	Relative to limit conditions
max	Relative to maximum values
ref	Relative to reference values
se	Relative to the Stirling engine
sp	Set-point
t	Relative to heat

1. INTRODUCTION

Buildings play an essential role in energy consumption, as they represent about 40% of the total final energy consumed in the European Union (EU), as well as 36% of the greenhouse gas emissions [1]. Consequently, adopting energy efficiency measures and promoting renewable energies is nowadays an indispensable aspect for accomplishing two of the three key targets included in the 2030 climate and energy framework (32.5% increase in the energy efficiency and 40% reduction of CO_2 emissions) [2] and on the path towards being climate neutral in 2050, as stated in the European 2050 long term strategy [3]. In this sense, as noted in

Directive 2012/27/EU on energy efficiency [4], recently corroborated in the Clean energy for all Europeans package through Directive (EU) 2018/844 [5], combined heat and power (CHP) in general and micro-CHP in particular, is a cornerstone for getting reductions in primary energy consumption and pollutant emissions in residential applications [6, 7]. Amongst the main technologies susceptible to being installed in single-family or small multi-family houses, the Stirling engine (SE) appears as an emerging technology which can provide those intrinsic benefits of micro-CHP, but also those attributable to the Stirling technology itself, such as multi-fuel capability [8] and low emissions, both from the acoustic and pollutant points of view [9].

However, despite all the research and development projects and studies which have been undertaken around this technology in the last few years –summarized in the review presented by Wang et al. [10]–, there are some technological challenges that must be overcome [11]. Additionally, it is worth noting that there is still a long way to go before it becomes competitive in the small residential sector, both technically (no full-length global testing has been conducted) and economically [12, 13]. Thus, beyond laboratory and field-test-based experimental research which are indispensable, simulation-based studies also become necessary. Specifically, these studies allow optimising the integration of SE within thermal plants [14] and the subsequent application to assess the energy, environmental and economic performance of actual applications under specific operating constraints (e.g., [15-17]), which will open up the possibility for providing improvements in their design, operation conditions and analysis.

A very exhaustive modelling review was presented by Kelly and Beausoleil-Morrison [18]. In this work, they revealed that, whereas several combustion engine-based models developed for general analysis exist in the literature (e.g., Dochat [19], Heywood [20]), small-scale cogeneration models addressed to building energy simulation tools are scarce. According to the classification of combustion engine-based models by Urieli and Berchowitz [21] –lately extended by Kelly and Beausoleil-Morrison [18]–, amongst parametric or zero-order, first-order, second-order and third-order models, most of the models available in the literature fall into the last two categories and were developed for the analysis of engine phenomena occurring over very short time scales.

In this sense, during the last few years, several works attempting to model the performance of Stirling engines have been presented, based on both thermodynamics [22, 23] or thermoacoustics [24]. Nevertheless, as mentioned by Valenti et al. [25], whereas detailed numerical models are especially useful for improving the designs of generation devices by evaluating the major sources of energy waste and optimizing geometries of both the engine and the heat exchangers, this is generally beyond the scope of building energy simulation (BES). On the contrary, BES is more sensitive to those energy aspects that relate the operation of a specific micro-CHP device with the rest of the components of the installation to be simulated, as well as the building

whose loads are to be met; thus reducing the need for a rigorous modelling of the complex processes taking place within.

Focusing on building-integrated combustion Stirling engine-based CHP modelling, Pearce et al. [26, 27] studied the annual performance of Stirling engines in comparison to measured and calculated residential heating loads by assuming constant seasonal efficiencies. This modelling approach neglected the effects of different control strategies and thermal storage, which are of great interest when investigating the integration of this technology in residential buildings.

Thiers et al. developed a black-box model for a wooden pellet-fuelled 3 kW_e Stirling unit [28]. Their approach, based on hourly intervals, consisted of a simplified parametric model using the information obtained through steady and dynamic tests carried out. Its quasi-static nature and, especially, the impossibility of calibrating the model for other Stirling units, were the main limitations of their approach. In the same vein, Conroy et al. developed and carried out a field trial data-based validation of an easily customizable dynamic energy model for a 1 kW_e and 8 kW_t Stirling engine [29]. The model developed was based on empirical equations which were specific to the engine under study. Thus, one of the main purposes of the work was to provide installers of the aforementioned engine with a tool to predict both thermal and electric outputs using the heat demand profile of a given dwelling, as well as for policy-makers to explore the sustainability of the micro-CHP unit in different house types for larger scale deployment. More recently, Uchman et al. presented a data-driven model for time-domain evaluation of a free-piston Stirling micro-CHP system [30]. The model, implemented in Matlab-Simulink, relied on measurements gathered during long-term operation with variable thermal load; nevertheless, due to its nature, the model is practically impossible to apply outside laboratory conditions.

Cacabelos et al. [31], as a continuation of a previous work [32], went for a different modelling approach. They developed a one-dimensional grey-box dynamic model of a commercial micro-CHP unit, consisting of two lumped masses and a heat exchanger, based on components from the TRNSYS libraries. Even though their modelling approach was very interesting, some of the proposed geometrical and operation parameters are generally hard to get from the manufacturers. The main weaknesses of the model were the lack of modelling of the fuel input, the neglect of heat losses to the surroundings, and the dynamic nature of the data sets used for calibration and validation.

Kelly and Beausoleil-Morrison [18] took a step forward in this area with the modelling approach developed under the working lines of the IEA's Annex 42, which aimed to predict the thermal and electrical outputs of the residential micro-CHP devices. Their semi-empirical model, which partially relied on experimental data, was developed with the aim of being used in conjunction with BES environments, and therefore, allowing the technical, environmental and economic performance of micro-CHP devices to be assessed within full-scale

simulation environments. Basically, this means that the model must interact with the rest of the model domains within the simulation project on the basis of a given time-step. This model presented important improvement margins, especially regarding transient phases and part-load operation. Lombardi et al. [33] reviewed the Annex 42 model and proposed some improvements and simplifications by means of a linear difference model based on experimentally determined linear coefficients and reference parameters. However, the full model was not validated.

Following the same modelling approach, in 2014, Bouvenot et al. presented a simpler semi-physical dynamic model of a gas-run micro-CHP boiler for its implementation in building-simulation environments, which was validated via experimental tests [34]. However, this model was only valid for non-modulating Stirling devices. It overlooked the fuel overshooting which takes place in this kind of devices during the warm-up period, and the validity range excluded typical temperatures in traditional radiator-based space heating systems.

In this paper, taking both the approaches of Kelly and Beausoleil-Morrison (with the subsequent improvements introduced by Lombardi et al.) and Bouvenot et al. as references, a BES-integrated dynamic semi-empirical grey box model for a natural gas-run micro-CHP boiler, whose primary mover is a SE, is developed. The main goal of the work is to improve the existing dynamic models of SE-based micro-CHP systems. As a novelty, the model herein presented enhances the analysis of the dynamics that occur during the start-up and cool-down periods, better approaches some steady physical phenomena while maintaining the simplicity required within BES environments and, unlike some other previous models, it also tackles the traditionally overlooked part-load performance of the system. Furthermore, the model is calibrated and validated for the whole temperature range that can be used in the domestic sector. To do so, a full characterization of a 1 kW_e Stirling boiler is also assessed. In this sense, the experimental test-bench developed, where the tested device could be implemented for its individual testing, is also introduced.

2. MODELLING APPROACH

A Stirling engine-based micro-CHP system is a primary energy conversion system which produces a simultaneous output of electricity and heat for domestic use. While the SE, i.e., the prime mover, drives the generator that produces electrical power, useful heat for space heating and DHW is obtained through a heat exchanger that recovers waste heat from both the engine casing and the combustion exhaust gases. Additionally, as depicted in Figure 1, many of the manufacturers of these micro-CHP units also include an auxiliary burner (AB), mounted on the heat exchanger, which operates when the heating demand is increased above the capacity of the main burner.

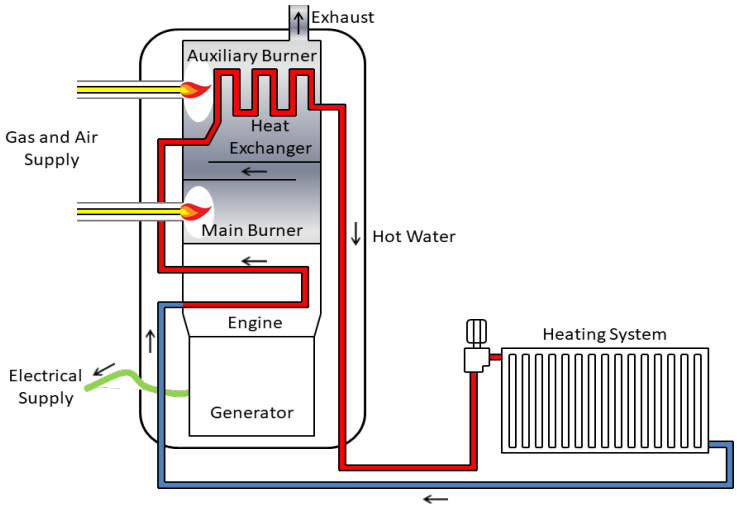

Figure 1 – Basic layout of a Stirling engine-based micro-CHP unit (adapted from [35]).

As discussed in section 1, a grey box modelling approach is proposed in this paper. Thus, the model is based on the general mass and energy conservation principles, supported by empirical expressions that rely on parametric factors that must be determined experimentally. In this way, the main objective of the model is to predict, semi-empirically, the main energy flows of SE-based micro-CHP devices –fuel consumption and electric and thermal productions– using the same approach for both generators, the SE and the AB, separately.

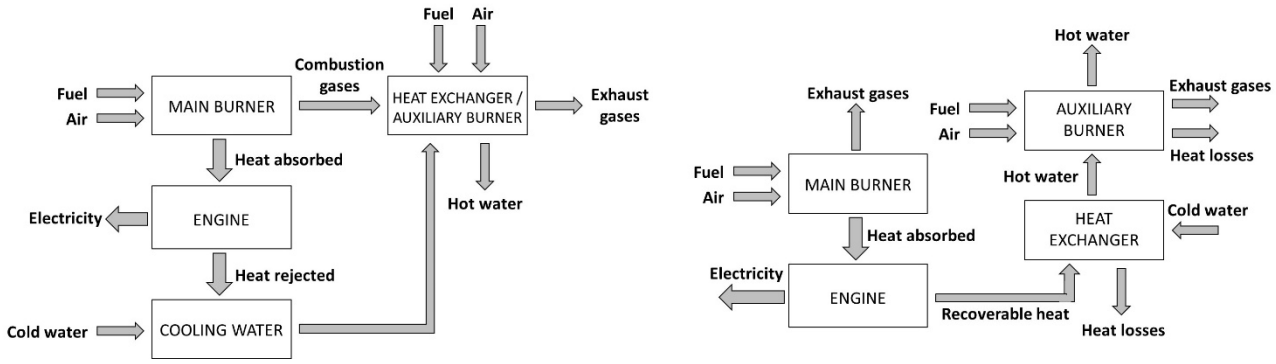

Figure 2 – Mass and energy flows of the Stirling micro-CHP unit: actual (left) and simplified (right).

Actual mass and energy flows taking place through an engine are schematized in Figure 2 (left). Nevertheless, for modelling purposes, these processes are reordered and the energy balance is posed as depicted in Figure 2 (right). Thus, heat absorbed from the engine and the exhaust gases in the heat exchanger are lumped together within an effective heat transfer process between the engine and the heat exchanger (recoverable heat), so simplifying the actual phenomena.

According to the aforementioned modelling topology, three control volumes (systems that exchange energy and mass) and a control mass (a system that only exchanges energy) were set out to model the dynamic thermal performance of the micro-CHP combi-boiler, as depicted in Figure 3:

- burner or head of the engine control volume,
- engine block control mass,
- heat exchanger control volume corresponding to the Stirling engine operation, and
- auxiliary burner control volume when extra heat is required.

All the components are supposed to be thermally defined by a unique mean temperature.

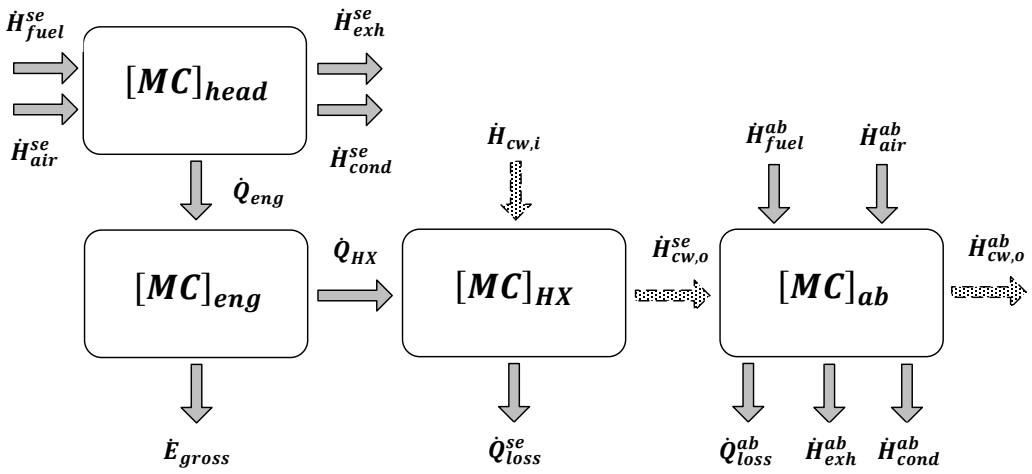

Figure 3 – Control mass and volumes used in the dynamic thermal performance modelling of the Stirling micro-CHP unit.

The head control volume represents the energy conversion of the energy contents of the external source (fuel) into gross heat in the form of exhaust gas, some of which is recovered and transferred to the engine control mass, where electricity is produced in the alternator. The general energy balance of this control volume can be written as follows:

$$[MC]_{head} \cdot \frac{dT_{head}}{dt} = \dot{H}^{se}_{fuel} + \dot{H}^{se}_{air} - \dot{H}^{se}_{exh} + \dot{H}^{se}_{cond} - \dot{Q}_{eng} \qquad \text{Equation 1}$$

where $[MC]_{head}$ is the thermal capacitance of the engine-head control volume; T_{head} is the mean temperature of the hot-side of the engine; $\dot{H}^{se}_{fuel}$ is the total enthalpy of the fuel input of the main burner; $\dot{H}^{se}_{air}$ is the enthalpy of the humid air used for the main combustion; $\dot{H}^{se}_{exh}$ is the enthalpy, including both the sensible and the latent, of the exhaust gas associated to the main burner; $\dot{H}^{se}_{cond}$ is the enthalpy of the recoverable latent heat of the exhaust gas; and $\dot{Q}_{eng}$ is the gross amount of heat rate recovered from the exhaust gases and transferred to the engine-block.

On the other hand, the energy balance of the engine-block control mass can be written as follows:

$$[MC]_{eng} \cdot \frac{dT_{eng}}{dt} = \dot{Q}_{eng} - \dot{E}_{gross} - \dot{Q}_{HX} \qquad \text{Equation 2}$$

where $[MC]_{eng}$ is the thermal capacitance of the engine control mass, where heat is converted into electricity; T_{eng} is the mean temperature of the engine; $\dot{E}_{gross}$ is the gross electric power output of the engine; and $\dot{Q}_{HX}$ is the net amount of heat rate recovered from the engine casing and the exhaust gases and transferred to the heat exchanger.

The heat exchanger control volume represents the heat transfer fluid flowing through the engine and the elements of the heat exchanger in direct thermal contact that take part of the heat fraction recovered from the exhaust gases. Thus, the thermal mass of this block considers both the capacitance of the heat exchanger itself, as well as that of the heat exchanger body associated to the engine block. The energy balance corresponding to this control volume can be written as follows:

$$[MC]_{HX} \cdot \frac{dT_{cw,o}^{se}}{dt} = \dot{Q}_{HX} - \dot{Q}_{loss}^{se} - \dot{Q}_{net}^{se} \qquad \text{Equation 3}$$

where $[MC]_{HX}$ is the thermal capacitance of the heat exchanger control volume, where the thermal recovery takes place; $T_{cw,o}^{se}$ is the mean temperature of the heat exchanger, which is considered to be representative of that of the cooling water at the outlet due to the logarithmic increase in the temperature of a cold fluid flowing through a heat exchanger; $\dot{Q}_{loss}^{se}$ is the heat loss rate through the surface of the micro-CHP engine, which is considered to occur from the cooling water to the surroundings; and $\dot{Q}_{net}^{se}$ is the net main thermal output of the micro-CHP unit, which stands for the enthalpy difference of the cooling water between the outlet and the inlet ($\dot{H}_{cw,o}^{se} - \dot{H}_{cw,i}$).

Meanwhile, the auxiliary burner block considers both the energy conversion of the energy contents of the second energy source and the thermal capacitance of the said element and its associated heat exchange between the exhaust and the cooling water. Since the thermal mass of the back-up boiler is already contained in the term of the heat exchanger, it is not taken into consideration when the auxiliary burner is off. Its energy balance corresponds to the following:

$$[MC]_{ab} \cdot \frac{dT_{cw,o}^{ab}}{dt} = \dot{H}_{fuel}^{ab} + \dot{H}_{air}^{ab} - \dot{H}_{exh}^{ab} + \dot{H}_{cond}^{ab} - \dot{Q}_{loss}^{ab} - \dot{Q}_{net}^{ab} \qquad \text{Equation 4}$$

where $[MC]_{ab}$ is the thermal capacitance of the auxiliary burner control volume, where the additional energy conversion takes place; $T_{cw,o}^{ab}$ is the mean temperature inside the additional boiler; $\dot{H}_{fuel}^{ab}$ is the total enthalpy of the fuel input of the additional burner; $\dot{H}_{air}^{ab}$ is the enthalpy of the humid air used for the additional combustion; $\dot{H}_{exh}^{ab}$ is the enthalpy of the exhaust gas associated to the additional burner; $\dot{H}_{cond}^{ab}$ is the enthalpy of the recoverable latent heat of the exhaust gas associated to the auxiliary burner; $\dot{Q}_{loss}^{ab}$ is the heat loss rate through the surface of the unit associated to the backup boiler; and $\dot{Q}_{net}^{ab}$ is the net additional thermal output of the micro-CHP unit ($\dot{H}_{cw,o}^{ab} - \dot{H}_{cw,o}^{se}$).

As previously mentioned, the model does not attempt to physically model the actual heat transfer phenomena taking place in micro-CHP units, but represents exhaust gases by heat transfer-rates between the main control mass and volumes. This approach considers that all the heat obtained from the combustion process is first addressed to the hot-side of the engine and, afterwards, it is the head of the engine which transfers heat to the engine-block. Finally, heat not absorbed by the thermodynamic power cycle, as well as that rejected, is partially transferred from the engine-block to the cooling water, taking into account the fact that heat losses to the ambient occur as well.

Heat transfer between the different control mass and volumes are modelled as the product of an effective UA coefficient and the temperature difference of the control mass and volumes. Thus, heat transferred from the combustion chamber to the engine block, as well as that from the engine to the heat exchanger, is modelled as follows:

$$\dot{Q}_{eng} = [UA]_{eng} \cdot \left(T_{head} - T_{eng}\right) \quad \text{Equation 5}$$

$$\dot{Q}_{HX} = [UA]_{HX} \cdot \left(T_{eng} - T_{cw,o}^{se}\right) \quad \text{Equation 6}$$

When the micro-CHP unit only works with the main burner, heat losses are exclusively those corresponding to the engine. Since cooling water flows by the outer side of the engine block, the model considers that it is the water which receives heat corresponding to losses of the engine and, therefore, it is the cooling water control volume that undergoes heat losses:

$$\dot{Q}_{loss}^{se} = [UA]_{loss}^{se} \cdot \left(T_{cw,o}^{se} - T_{amb}\right) \quad \text{Equation 7}$$

Finally, concerning heat losses when the auxiliary burner is running, $\dot{Q}_{loss}^{ab}$, as stated for the SE, it is considered that losses to the surroundings also correspond to the cooling water. Additionally, since the auxiliary burner will not normally operate unless the main burner is on, no losses through the jacket of the engine, or towards the head of the engine, are explicitly associated to the additional boiler:

$$\dot{Q}_{loss}^{ab} = [UA]_{loss}^{ab} \cdot \left(T_{cw,o}^{ab} - T_{amb}\right) \quad \text{Equation 8}$$

2.1.Steady operation

Under steady-state conditions, the fuel input and the electric and thermal power productions can be modelled using correlations that relate them to the cooling water return temperature, $T_{cw,i}$, and the cooling water mass flow, $\dot{m}_{cw}$. Since this kind of devices are often capable of modulating their thermal output, the partial load performance, in terms of the thermal load fraction, α_t, also affects the definition of these correlations.

2.1.1. Thermal power

The thermal output of a SE unit under steady conditions depends on three operational ranges. First, when the thermal demand exceeds the maximum heat output of the unit at a given mass flow and return temperature conditions, i.e., when the temperature of the cooling water at the outlet of the engine, $T_{cw,o}^{se}$, is below the generation set-point temperature, $T_{cw,o}^{sp}$, the engine will work at full load in order to reach that set-point.

Second, once the set-point temperature is reached, the engine burner will start modulating so that the thermal production can be adapted to the demand. Consequently, a part-load ratio, α_t^{se}, must be defined as the relation between the instantaneous thermal power and the nominal full-load power at those mass flow and cooling water return conditions, which is used afterwards for modelling the electric and fuel performances.

Finally, the model must also take into consideration the maximum modulation rate, i.e., the minimum thermal power the engine can provide, below which, with the corresponding hysteresis, the engine will turn off.

$$\dot{Q}_{net}^{se} = \begin{cases} \dot{Q}_{net,full}^{se} & \text{for } T_{cw,o}^{max} \leq T_{cw,o}^{sp} \\ \dot{Q}_{net,part}^{se} & \text{for } T_{cw,o}^{min} - \Delta T < T_{cw,o}^{sp} < T_{cw,o}^{max} \\ 0 & \text{for } T_{cw,o}^{min} \geq T_{cw,o}^{sp} + \Delta T \end{cases} \qquad \text{Equation 9}$$

where $T_{cw,o}^{max}$ and $T_{cw,o}^{min}$ are the outlet temperature of the cooling water at full load and minimum load operation, respectively; and ΔT is the internally controlled temperature hysteresis for the outlet cooling water before the engine turns off. This makes the engine turn off once the actual outlet temperature exceeds the set-point on certain pre-fixed degrees.

The resulting net heat recovery of the cooling water can be determined by means of the thermal energy transport equation:

$$\dot{Q}_{net}^{se} = \dot{m}_{cw} \cdot c_{cw} \cdot \left(T_{cw,o}^{se} - T_{cw,i}\right) \qquad \text{Equation 10}$$

where $\dot{Q}_{net}^{se}$ is the net thermal production of the micro-CHP unit; $\dot{m}_{cw}$ is the cooling water mass flow; c_{cw} is the specific heat of the cooling water; and $T_{cw,o}^{se}$ and $T_{cw,i}$ are the respective temperatures of the cooling water at the outlet and inlet of the micro-CHP unit.

Solving Equation 1, Equation 2 and Equation 3, together with Equation 10, the cooling water outlet temperature ($T_{cw,o}^{se}$) is obtained. If the set-point temperature ($T_{cw,o}^{sp}$) exceeds the value of $T_{cw,o}^{se}$, the thermal

load fraction will be equal to 1 and the engine will be operating at full load; otherwise, the burner will start modulating and the part-load operation will start.

The thermal load fraction, α_t^{se}, which is dependent on the production set-point temperature, is obtained as the quotient of the actual heat demand and the maximum heat producible at the same cooling water mass flow and inlet temperature conditions.

$$\alpha_t^{se} = \frac{\dot{Q}_{net,sp}^{se}}{\dot{Q}_{net,max}^{se}} \quad \text{Equation 11}$$

where $\dot{Q}_{net,sp}^{se}$ is the net thermal output when the temperature of the cooling water at the outlet is at the set-point and $\dot{Q}_{net,max}^{se}$ is the maximum net heat power to be transferred to the cooling water at certain cooling water temperature and flow conditions. The determination of $\dot{Q}_{net,max}^{se}$ can be assessed by means of a multiple linear regression parametric equation. This multiple linear approach, based on the regression philosophy and considerations first proposed by Lombardi et al. [33] and later modified by Bouvenot et al. [34], evinces that an energy exchange or efficiency can be expressed as a function of a reference value, with its corresponding cooling water inlet temperature and mass flow, and the actual water temperature and mass flow.

$$\dot{Q}_{net,sp}^{se} = \dot{m}_{cw} \cdot c_{cw} \cdot \left(T_{cw,o}^{sp} - T_{cw,i}\right) \quad \text{Equation 12}$$

$$\dot{Q}_{net,max}^{se} = \dot{Q}_{net,ref}^{se} + a_1^{se} \cdot \left(T_{cw,i} - T_{cw,i}^{ref,se}\right) + a_2^{se} \cdot \left(\dot{m}_{cw} - \dot{m}_{cw}^{ref,se}\right) \quad \text{Equation 13}$$

where a_1^{se} and a_2^{se} are empirically determined regression coefficients and $\dot{Q}_{net,ref}^{se}$ is the full-load thermal power value, measured when the respective temperature and mass flow of the cooling water are $T_{cw,i}^{ref,se}$ and $\dot{m}_{cw}^{ref,se}$.

Some devices are provided with an overheating protection control that, having once reached a certain level of cooling water temperature, reduces the power input, even if working at full-load. Consequently, somehow, the thermal load fraction is reduced to below 1. For those cases when the engine fulfils full-load conditions and the cooling water temperature, $T_{cw,i}$, is above the limit temperature above which the thermal power is reduced, $T_{cw,i}^{lim}$, the following correction is proposed:

$$\alpha_t^{se} = 1 - a_3^{se} \cdot \left(T_{cw,i} - T_{cw,i}^{lim}\right) + a_4^{se} \cdot \left(\dot{m}_{cw} - \dot{m}_{cw}^{ref,se}\right) \quad \text{Equation 14}$$

Considering that some micro-CHP units include both the Stirling engine and an additional boiler, as well as a variable-speed pump, independent nominal values for the engine will not always be available in the manufacturer's data sheets. Consequently, the proposed reference conditions are identified by those

obtained through experimental evaluation under nominal volumetric flow conditions, which normally correspond to the first stage of the internal pump at which the SE operates. For full load reference values, the nominal power is assumed for the most favourable return temperature, i.e., 30 °C.

Since the auxiliary burner is also modulating, the previously presented modelling fundamentals can be applied to the additional boiler. Thus, its thermal load fraction, α_t^{ab}, can be expressed as follows:

$$\alpha_t^{ab} = \frac{\dot{Q}_{net,sp}^{ab}}{\dot{Q}_{net,max}^{ab}} \qquad \text{Equation 15}$$

where the actual heat demand, $\dot{Q}_{net,sp}^{ab}$, and the maximum heat producible by the auxiliary burner at some given cooling water temperature and flow conditions, $\dot{Q}_{net,max}^{ab}$, are determined as follows:

$$\dot{Q}_{net,sp}^{ab} = \dot{m}_{cw} \cdot c_{cw} \cdot \left(T_{cw,o}^{sp} - T_{cw,o}^{se}\right) \qquad \text{Equation 16}$$

$$\dot{Q}_{net,max}^{ab} = \dot{Q}_{net,ref}^{ab} + a_1^{ab} \cdot \left(T_{cw,o}^{se} - T_{cw,i}^{ref,ab}\right) + a_2^{ab} \cdot \left(\dot{m}_{cw} - \dot{m}_{cw}^{ref,ab}\right) \qquad \text{Equation 17}$$

2.1.2. Electric power

As SE devices are typically regulated in order to reach and maintain a certain level of electric output, the modelling is tackled in terms of net power by a multiple linear regression correlation. Since the performance of any power cycle depends on the temperature of a hot and a cold reservoir, the correlation proposed considers the net power variation as a function of the temperature of the head of the engine (hot reservoir) and the inlet temperature and mass-flow of the cooling water (cold reservoir). As the temperature of the hot side will decrease once the firing rate is reduced, this temperature, which is usually reported by its control and monitoring system, allows both full and part load operation to be encompassed through a unique correlation.

$$\dot{E}_{net}^{se} = \dot{E}_{net,ref}^{se} + b_1^{se} \cdot \left(T_{head} - T_{head}^{ref}\right) + b_2^{se} \cdot \left(T_{cw,i} - T_{cw,i}^{ref,se}\right) + \\ + b_3^{se} \cdot \left(\dot{m}_{cw} - \dot{m}_{cw}^{ref,se}\right) \qquad \text{Equation 18}$$

where $\dot{E}_{net}^{se}$ is the actual net electric power at full load; $\dot{E}_{net,ref}^{se}$ is the reference net electric power; T_{head} is the temperature of the burner; and T_{head}^{ref} is the reference temperature of the head of the engine which constitutes the hot reservoir of the cycle.

While the net electric power can be measured through an external electricity meter, the gross electric power, $\dot{E}_{gross}$, can generally be obtained through an internal measurement reported by its control and monitoring

system. Thus, the electric consumption requirements of the device can be determined as a difference of both:

$$\dot{E}_{gross} = \dot{E}_{net}^{se} + \dot{E}_{standby} + \dot{E}_{fan}^{se} + \dot{E}_{pump}^{se} \quad \text{Equation 19}$$

The electric consumption considers, on the one hand, the standby consumption ($\dot{E}_{standby}$) mainly due to the electronic control board and, on the other, the energy required by the auxiliaries, i.e., the intake air fan ($\dot{E}_{fan}^{se}$) and the cooling water circulation pump ($\dot{E}_{pump}^{se}$).

However, as the final purpose of the modelling presented in this article is to implement it in a building simulation tool, the pump consumption is excluded from these parasitic losses. So, when a simulation is done, if an external pump is to be used instead of the internal one, its energy consumption can be accounted independently and it can then be put together with the net power production extracted from Equation 18. Additionally, since the engine may operate together with the auxiliary burner, accounting for the energy consumption of the pump separately permits this consumption to be distributed between the two generators.

Concerning the auxiliary burner, since it does not produce any electricity but only consumes it, its net electricity exchange is expressed as follows:

$$\dot{E}_{net}^{ab} = -\dot{E}_{fan}^{ab} - \dot{E}_{pump}^{ab} \quad \text{Equation 20}$$

where $\dot{E}_{fan}^{ab}$ and $\dot{E}_{pump}^{ab}$ stand for the electricity consumption of the fan and the pump that is directly related to the operation of the auxiliary burner, respectively.

2.1.3. Fuel power

The fuel input, in terms of power, is related to the fuel volumetric flow as follows:

$$\dot{F} = \dot{V}_f \cdot LHV_f \quad \text{Equation 21}$$

where $\dot{V}_f$ is the volumetric fuel flow, in m^3/h; and LHV_f is the lower heating value of the fuel, in kWh/m^3.

Even though the hourly variations of the fuel composition is commonly not known, the daily higher and lower heating values, as well as the specific density, are usually given by gas distribution companies. In this case, the enthalpies of all the terms concerning fuel and air inputs ($\dot{H}_{fuel}$ and $\dot{H}_{air}$) and the exhaust enthalpy ($\dot{H}_{exh}$), as well as the corresponding condensed fraction of the exhaust gases ($\dot{H}_{cond}$), can be joined together within a combustion efficiency term, thus avoiding an exhaustive analysis of the combustion. This combustion

efficiency, η_{comb}, together with the fuel power input related to the LHV, $\dot{F}$, takes into consideration the power fluxes which also imply some mass transfer (fuel input, air, exhaust, condensate):

$$\eta_{comb} \cdot \dot{F} = \dot{H}_{fuel} + \dot{H}_{air} - \dot{H}_{exh} + \dot{H}_{cond} \quad \text{Equation 22}$$

This efficiency can be modelled by a multiple linear regression approach, such as that used for the maximum thermal power output, thus avoiding the necessity to know variations in the fuel composition. This approach considers that the efficiency can be expressed as a function of a reference efficiency value, η_{comb}^{ref}, associated to the corresponding cooling water inlet reference temperature ($T_{cw,i}^{ref}$) and mass flow ($\dot{m}_{cw}^{ref}$), and the actual water temperature and mass flow, as follows:

$$\eta_{comb}^{se} = \eta_{comb,ref}^{se} + c_1^{se} \cdot \left(T_{cw,i} - T_{cw,i}^{ref,se}\right) + c_2^{se} \cdot \left(\dot{m}_{cw} - \dot{m}_{cw}^{ref,se}\right) \quad \text{Equation 23}$$

Considering all this, the gross heat obtained from the combustion, under steady-state conditions, can be obtained as follows:

$$\dot{Q}_{comb} = \eta_{comb} \cdot \dot{F} \quad \text{Equation 24}$$

where $\dot{Q}_{comb}$ is the gross heat obtained from the combustion, which accounts for the difference between the enthalpies of the input flows (fuel and combustion air) and that of the exhaust gases.

These engines are generally regulated to maintain some pre-set temperature conditions at the hot-side of the engine, i.e., the head of the engine, which enable the desired electric output to be reached. To do so, the intake air mass flow is regulated by the fan rotation speed and the fuel mass flow accordingly. Therefore, the fuel flow can vary depending on the LHV, and a certain power input is required to reach the desired operation point. Thus, the fuel consumption in nominal conditions under steady operation, $\dot{F}_{nom}^{se}$, is related to the net electrical power by means of the electric efficiency:

$$\dot{F}_{nom}^{se} = \frac{\dot{E}_{net}^{se}}{\eta_{e,nom}^{se}} \quad \text{Equation 25}$$

where $\eta_{e,nom}^{se}$ and $\dot{E}_{net}^{se}$ are, respectively, the nominal electric efficiency and the net electric output when the engine operates at full load.

For its part, the nominal net electric efficiency is modelled in terms of a multiple linear regression correlation:

$$\eta_{e,nom}^{se} = \eta_{e,ref}^{se} + d_1^{se} \cdot \left(T_{cw,i} - T_{cw,i}^{ref,se}\right) + d_2^{se} \cdot \left(\dot{m}_{cw} - \dot{m}_{cw}^{ref,se}\right) \quad \text{Equation 26}$$

Combining Equation 18 and Equation 26, as established in Equation 25, the nominal fuel power at full load is determined.

On the other hand, when the micro-CHP unit works at part load, since the burner modulates its firing rate in order to achieve the generation set point temperature, a linear relationship between the thermal load and the firing rate is proposed:

$$\alpha_f^{se} = 1 - e^{se} \cdot (1 - \alpha_t^{se}) \quad \text{Equation 27}$$

where α_f^{se} is the firing rate of the burner and e^{se} is an empirical coefficient.

Finally, in order to impose the modulation limits of the devices, a minimum firing rate must be defined that makes the device switch off once this limit is surpassed. This minimum firing rate, for the case of the SE, is generally related to the temperature of the head of the engine, so that when this temperature drops below a certain prefixed minimum value, $T_{head,min}$, the unit will shut-down.

Taking all this into account, the actual fuel power of the SE, $\dot{F}_{se}$, is determined as follows:

$$\dot{F}_{se} = \begin{cases} \alpha_f^{se} \cdot \dot{F}_{nom}^{se} & \text{for } T_{head} \geq T_{head,min} \\ 0 & \text{for } T_{head} < T_{head,min} \end{cases} \quad \text{Equation 28}$$

With respect to the AB, due to the difference between its control and that of the SE, the modelling of the fuel consumption is approached in a different way, except for the combustion efficiency.

In this sense, the fuel input power in nominal conditions is related to the maximum heat output achievable (previously defined through Equation 17):

$$\dot{F}_{nom}^{ab} = \frac{\dot{Q}_{net,max}^{ab}}{\eta_{t,nom}^{ab}} \quad \text{Equation 29}$$

where $\eta_{t,nom}^{se}$ is the nominal thermal efficiency when the auxiliary burner operates at full load. This nominal net thermal efficiency is modelled in terms of a multiple linear regression correlation:

$$\eta_{t,nom}^{ab} = \eta_{t,ref}^{ab} + d_1^{ab} \cdot \left(T_{cw,i} - T_{cw,i}^{ref,ab}\right) + d_2^{ab} \cdot \left(\dot{m}_{cw} - \dot{m}_{cw}^{ref,ab}\right) \quad \text{Equation 30}$$

On the other hand, analogous to the SE, a linear relationship between the thermal load and the firing rate is proposed to define the part-load performance:

$$\alpha_f^{ab} = 1 - e^{ab} \cdot \left(1 - \alpha_t^{ab}\right) \quad \text{Equation 31}$$

where α_f^{ab} is the firing rate of the auxiliary burner and e^{ab} is an empirical coefficient.

Additionally, concerning the part-load performance, contrary to the main burner, the auxiliary burner does not have a control temperature signal that limits modulation. In this case, the maximum modulation rate is defined with respect to the thermal output, as follows:

$$\alpha_{t,min}^{ab} = \frac{\dot{Q}_{net,min}^{ab}}{\dot{Q}_{net,nom}^{ab}} \quad \text{Equation 32}$$

where $\dot{\boldsymbol{Q}}_{\boldsymbol{net,min}}^{\boldsymbol{ab}}$ and $\dot{\boldsymbol{Q}}_{\boldsymbol{net,nom}}^{\boldsymbol{ab}}$ are, respectively, the minimum and maximum thermal power provided by the auxiliary burner in steady operation, which can be experimentally determined.

Taking all this into account, the fuel power of the AB, $\dot{F}_{ab}$, is determined as follows:

$$\dot{F}_{ab} = \begin{cases} \alpha_f^{ab} \cdot \dot{F}_{nom}^{ab} & \text{for } \alpha_t^{ab} \geq \alpha_{t,min}^{ab} \\ 0 & \text{for } \alpha_t^{ab} < \alpha_{t,min}^{ab} \end{cases} \quad \text{Equation 33}$$

2.2. Transient operation

The transient thermal behaviour of the generator is characterized by the thermal capacity of both the engine block and the working fluid, the internal heat exchanger and the external combustor. The energy exchanges that take place during the operation modes described below can be determined by solving the specific equations subsequently defined for each operation mode, together with Equation 1, Equation 2, Equation 3 and Equation 4.

2.2.1. Stand-by

Since SE-based micro-CHP units are generally thermally driven devices, when no heat is requested, no activation signal is transferred to the electronic control unit (ECU) and the unit remains in stand-by. Under this mode of operation, the unit does not consume any fuel or produce any heat or electricity. Nevertheless, since the ECU is permanently active in order to respond to an activation request, some electricity is required for these electronic controllers. Thus, during the standby-mode, the following equations govern the performance of the unit:

$$\dot{m}_{fuel} = \dot{m}_{fuel,standby} = 0 \quad \text{Equation 34}$$

$$\dot{Q}_{net} = \dot{Q}_{net,standby} = 0 \quad \text{Equation 35}$$

$$\dot{E}_{gross} = \dot{E}_{gross,standby} = 0 \quad \text{Equation 36}$$

$$\dot{E}_{net} = \dot{E}_{gross,standby} - \dot{E}_{net,standby} \quad \text{Equation 37}$$

where $\dot{E}_{net,standby}$ is the power required by the ECU while awaiting activation during the stand-by mode.

These four equations are applicable to both the prime mover (SE) and the AB.

Since, under standby mode, the fan and the pump are switched off, the effective heat transfer coefficients (Equation 5, Equation 6 and Equation 7) correspond only to natural convection. Thus, they will significantly differ from those associated to steady operation, where forced convection is the predominant heat transfer mechanism.

$$UA_{eng} = UA_{eng_{standby}}$$ Equation 38

$$UA_{HX} = UA_{HX_{standby}}$$ Equation 39

$$[UA]^{se}_{loss} = [UA]^{se}_{loss_{stanby}}$$ Equation 40

Concerning the AB, the model is structured so that, whenever it is off, no losses or thermal mass exist, and all the losses and inertia of the heat exchanger are exclusively associated to the heat exchanger control volume of the engine.

2.2.2. Warming-up

The warm-up process differs from one energetic vector to another. Once the engine receives the activation signal and it is switched on, the fan starts introducing air into the burner and the head of the SE is heated up until its temperature is high enough to make the piston move and, therefore, the generator starts producing electricity. As this process must be as fast as possible, the fuel consumption during this phase grows exponentially and exceeds the nominal value required during the steady-state operation.

During this period, three phases can be distinguished. First, when the combustion process starts, in order to raise the temperature of the head of the engine, no effective heat or electricity production takes place. Then heat production starts once the thermal mass of the heat exchanger reaches a high enough temperature to warm up the cooling water. It is not until the head of the SE gets a pre-set set-point temperature that electricity production begins.

Concerning fuel consumption, two main phases can be distinguished. First, as previously mentioned, once the engine switches on, the fuel consumed grows exponentially until the head of the engine reaches a pre-set temperature, achieving a peak. Then, the consumption drops smoothly until its value achieves that of the steady operation.

As stated before, the start-up fuel consumption during the warm-up period, on a mass basis, is modelled as a function of the steady-state value and the relationship between the actual head temperature and the nominal head temperature at which the fuel peak occurs:

$$\dot{m}_{f,warmup}^{se} = \begin{cases} \dot{m}_{f,max}^{se} \cdot \left(1 - e^{-\frac{T_{head}}{k_{f,1} \cdot T_{head,nom}^{start}}}\right) & \text{for } T_{head} < T_{head,nom}^{start} \\ \dot{m}_{f,warmup,2}^{se} & \text{for } T_{head} \geq T_{head,nom}^{start} \end{cases} \quad \text{Equation 41}$$

where $\dot{m}_{f,max}^{se}$ is the maximum fuel mass flow during the warm-up, i.e., the nominal fuel flow at the given cooling water mass flow and temperature conditions multiplied by an overshooting factor; $k_{f,1}$ is an empirical coefficient indicative of the sensitivity of the fuel power to the temperature of the head of the engine; and $\dot{m}_{f,warmup,2}^{se}$ is the fuel consumption from the moment the peak consumption is achieved until the warm-up phase ends. This latter term, which aims to reproduce the typically underdamped control of the gas valve, is determined as follows:

$$\dot{m}_{f,warmup,2}^{se} = \dot{m}_{f,nom}^{se} + \left[\left(\dot{m}_{f,max}^{se} - \dot{m}_{f,nom}^{se}\right) + k_{f,2} \cdot \frac{T_{eng} - T_{eng}^{start}}{T_{eng,nom} - T_{eng}^{start}}\right] \cdot exp\left(-k_{f,3} \cdot \frac{T_{eng} - T_{eng}^{start}}{T_{eng,nom} - T_{eng}^{start}}\right) \quad \text{Equation 42}$$

where $k_{f,2}$ and $k_{f,3}$ are empirical coefficients indicative of the sensitivity of the fuel power to the temperature of the engine control mass.

Since the objective of such control is to adapt the electric power output to its nominal value while at the same time maintaining security conditions, the fuel mass flow is related to the temperature of the engine control mass, which is responsible for determining whether the warm-up phase is completed or not.

With respect to the net electricity production during the warm-up phase:

$$\dot{E}_{net}^{se} = \begin{cases} -\left(\dot{E}_{standby} + \dot{E}_{fan}^{se}\right) & \text{for } T_{head} < T_{start}^{e} \\ \dot{E}_{net,nom}^{se} \cdot \left[1 - k_{e,1} \cdot \left(T_{eng,nom} - T_{eng}\right)\right] & \text{for } T_{head} \geq T_{start}^{e} \end{cases} \quad \text{Equation 43}$$

where $\dot{E}_{net,nom}^{se}$ is the net electricity power production at steady operation and $k_{e,1}$ is an empirical coefficient indicative of the sensitivity of the electric power during warm-up to the temperature of the engine control volume.

Regarding the effective heat transfer coefficients, no distinction is made between steady operation and warm-up periods, because the phenomena behind these heat transfer processes between control volumes can be treated in similar terms.

As for the auxiliary burner, once switched on, the fuel power rises to nominal conditions, while the net electric energy consumption is the same as in steady-state conditions.

2.2.3. Shutting-down

Once the stop signal is transferred to the device, the fuel supply is immediately cut off. However, the device continues to produce both electric and thermal energy during the shut-down period, where different stages can be distinguished.

$$\dot{m}_f = \dot{m}_{f\,shutdown} = 0 \qquad \text{Equation 44}$$

Concerning electricity production, once the engine is switched off, even though its value drops quickly, it continues to be active, due to the inertia of the engine, until the temperature of the hot side of the engine falls below a certain value (T^e_{stop}). Thus, the electricity output during this period is modelled through a 3-stretches equation:

$$\dot{E}^{se}_{net} = \begin{cases} \dot{E}_{net,shut-down} & \text{for } T_{head} > T^e_{stop} \\ -\left(\dot{E}_{standby} + \dot{E}_{fan} + \dot{E}_{pump}\right) & \text{for } T^t_{stop} < T_{head} \leq T^e_{stop} \\ -\dot{E}_{standby} & \text{for } T_{head} \leq T^t_{stop} \end{cases} \qquad \text{Equation 45}$$

where T^t_{stop} is the head temperature below which thermal production ceases; and $\dot{E}_{net,shutdown}$, is the net electricity production during the first part of the shut-down process, which can be calculated through Equation 46:

$$\dot{E}_{net,shutdown} = \dot{E}_{gross,shutdown} - \left(\dot{E}_{standby} + \dot{E}_{fan} + \dot{E}_{pump}\right) \qquad \text{Equation 46}$$

The gross electricity production during the first part of the shut-down, $\dot{E}_{gross,shutdown}$, is modeled through a linear equation, as follows:

$$\dot{E}_{gross,shutdown} = k_{e,2} \cdot \left(T_{head} - T^e_{stop}\right) \qquad \text{Equation 47}$$

where $k_{e,2}$ is an empirical coefficient indicative of the sensitivity of the fuel power to the temperature of the head of the engine.

The thermal production during the shut-down period takes place due to the fact that, even though the fuel supply is cut off, the fan of the device keeps on working and introducing air to the burner. So it continues to be heated up with the heat stored within the body of the engine, transferring such heat to the heat transfer fluid through the heat exchanger prior to its expulsion through the exhaust duct.

Generally, these devices are provided with an internal control that, once the temperature of the hot side of the engine drops below a certain pre-fixed value, T_{stop}^{t}, makes both the fan and the circulation pump stop and so cease heat production. However, if an external pump is used, the recovery of the heat stored within the engine can be stretched out. However, since the fan is already stopped, the heat recovered will be mainly that stored within the heat exchangers. This heat recovery can be determined by simultaneously solving Equation 1, Equation 2 and Equation 3.

On the other hand, micro-CHP units may be stopped through and external stop signal or halt due to high temperature protection. In these cases, before the engine switches to standby mode, an activation signal may be sent to the device, but it does not generally restart operation until the whole shut-down process has been completed.

As far as effective heat transfer processes between control mass and volumes are concerned, once the shutdown period starts, as mentioned, the fuel consumption is cut off; consequently, no exhaust gases flow through the device, only air. During this phase, the fan is on and the air-to-fuel ratio is generally very high, i.e., no significant change in the mass flow is appreciated. Nevertheless, since it is the working fluid of the thermodynamic cycle which is responsible for absorbing heat from the hot reservoir (head control volume) and rejecting it to the cold source (heat exchanger control volume), $[UA]_{HX}$ and $[UA]_{eng}$ must necessarily differ from those proposed for warm-up and steady operation modes. This is mainly due to the speed at which the engine moves in each phase and, once the engine is switched off, the velocity of the working fluid of the cycle decreases with respect to the aforementioned modes of operation.

$$UA_{eng} = UA_{eng_{shutdown}}$$ Equation 48

$$UA_{HX} = UA_{HX_{shutdown}}$$ Equation 49

In the case of the AB, once switched off, the fuel input is cut off as well as the air-intake fan. At this point, the internal pump continues to function, at a lower speed when internal controlled pumps are used, until the temperature difference between the outlet and the inlet of the cooling water drops below a certain value. However, since the AB is usually used as a backup of the SE, once no thermal support of the additional boiler is required, its burner will stop, but the pump and the fan will keep on working normally for the SE operation.

3. EXPERIMENTAL EVALUATION

According to the specifications and requirements previously defined for the modelling, a testing routine to obtain the required data for calibrating and validating the model was developed. These tests were developed in a versatile experimental facility sited at the Laboratory for Quality Control in Buildings (LCCE) of the Basque

Government [36], so that all the phenomena and conditions could be controlled and evaluated. Further information of the definition, scope and potential of this installation can be found in [37] and [38].

The unit chosen for this study was the Remeha eVita, which is a wall-mounted natural gas-run Stirling engine-based boiler. It is made of a linear free-piston Stirling engine manufactured by Microgen (MEC), which provides 5 kW_t and 1 kW_e for base loads, and an additional burner for peak loads of up to 23 kW_t. Both burners are condensing and modular. To characterize both the Stirling engine and the auxiliary boiler, the micro-CHP device was integrated within the installation as detailed in the simplified hydraulic diagram in Figure 4.

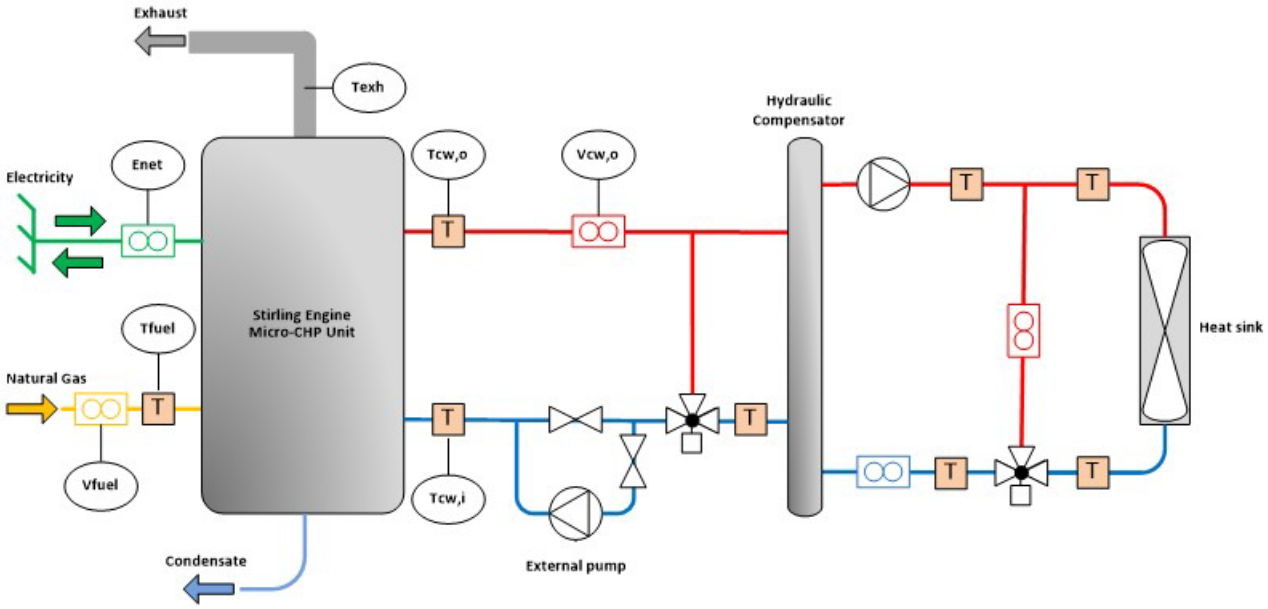

Figure 4 – Simplified hydraulic principle diagram of the Stirling engine test rig.

In order to maintain a constant return temperature of the cooling water and, consequently, reach steady-state conditions to study the influence this temperature has on the final performance of the micro-CHP unit, a three-way valve was disposed. Additionally, to be able to govern the cooling water mass flow and test different flow-rates, the internal pump of the boiler was disabled and a 3-stage external pump was installed.

Based upon previous experimental research and the need to tune-up the model presented before, the low-uncertainty measure points specified in Table 1 and described below were projected.

In order to determine the main energy flows accurately, several low-uncertainty gauges were set up around the Stirling device, as schematized in Figure 4.

Thus, apart from measuring both gross and net electricity productions, as well as the fuel consumption, PT-100 resistance temperature detectors and electro-magnetic flow meters were installed to determine the thermal power produced.

Table 1 – Summary of the main variables measured

Variable group	Measure	Symbol	Measuring description	Units
Electricity	Net power	$\dot{E}_{net}$	Input and output power measured with an electricity meter	W
	Gross power	$\dot{E}_{gross}$	Internal measurement	W
Natural gas	Volumetric flow	$\dot{V}_f^{\circ}$	Fuel flow in normal conditions measured with a gas counter	Nm³
	Temperature	T_{fl}	Measured with a thermo-hygrometer	°C
	Pressure	p_f	Measured with a manometer	mbar
	LHV	LHV_f°	Measurements and information of the gas distributor[1]	kWh/ Nm³
Ambient features	Temperature	T_{amb}	Measured with a thermo-hygrometer	°C
	Relative humidity	p_{amb}		%
Water circuit	Inlet temperature	$T_{cw,i}$	Measured with thermocouples	°C
	Outlet temperature	$T_{cw,o}$		°C
	Volumetric flow	$\dot{V}_{cw,o}$	Measured with an electromagnetic flow-meter	l/h
Exhaust gas	Volumetric flow	$\dot{V}_{exh}$	Measured with a gas analyzer	l/min
	Temperature	T_{exh}		°C
	Pressure	p_{exh}		hPa
	Composition			% / ppm
Others	Engine-head temperature	T_{head}	Internal measurement	°C

In relation to the fuel consumption, the power required by the device was determined, from reading the experimental dry-system counter installed, and the heating capacity of the fuel, both in normal conditions.

The electric power was measured by an electricity meter which allows the net electricity produced by the Stirling engine to be determined, as well as the consumption of the auxiliaries of the unit and the unit in stand-by mode itself.

Additionally, due to the impossibility of getting information concerning the functioning of the unit by means of external measurements, information from some internal variables measured by the unit for its own regulation were used. This information was acquired using a communication interface by Siemens between

[1] The natural gas composition was not measured straightaway in the laboratory. Continuous measurements were carried out nearby and the LHV obtained with those compositions was checked and compared to that provided by the gas distribution company for the station which feeds the laboratory.

the micro-CHP unit and the PC where all other data from the PLC were collected. Thus, the values of the temperature of the hot-side of the engine, as well as the gross electricity output, amongst other measurements, could be obtained.

Each of the three aforementioned energy input and outputs is obtained through the use of high precision instrumentation. Despite this high precision, every measurement involves an uncertainty that is reflected in the final calculation of energy flows (Table 2). Such global uncertainty was evaluated according to the Guide to the Expression of Uncertainty in Measurement [39]. Relative uncertainties, summarized in Table 2 for fuel, electric and thermal powers, give rise to uncertainties of 5.02%, 5.12% and 7.17% for thermal, electric and overall efficiencies, respectively. These uncertainties are mainly due to the high uncertainty associated to the natural gas LHV measurement.

Table 2 – Uncertainties associated to the main energy measurements.

Assessed Magnitude	Type of measurement	Measured magnitude	Instrumentation	Uncertainty	Total Uncertainty (%)
Fuel power	Indirect	Volumetric Flow	High precision flow meter	±0.5%	±5.02
		LHV	Provided by the gas company	±5%	
Electric power	Direct	Active power	CIRCUTOR CVM-1D-RS-485-C network analyzer	±1.00	±1.00
Thermal power	Indirect	Cooling water flow rate	MJK MagFlux flow meter	±0.1%	±0.17
		Inlet and outlet water temperature	PT100 1/10	±0.1%	
Electric efficiency	Indirect	-	-	-	±5.12
Thermal efficiency	Indirect	-	-	-	±5.02
Overall efficiency	Indirect	-	-	-	±7.17

4. MODEL CALIBRATION

In this section, characterization results of experimental tests carried out on the previously mentioned Remeha eVita device are presented for the subsequent calibration and validation of the model. These experimental tests took place from July 2016 to January 2017 in the experimental facility of the LCCE.

4.1.Parameter identification of the Stirling engine

The identification procedure encompasses the four main operating modes previously defined: steady operation, warm-up, shutdown and standby. Calibration tests were both steady and transient, depending on the parameter to be identified.

The parameters to be identified, previously introduced in the description of the model, can be classified into three main categories:

- Parameters of the performance map, which are related to the normal steady operation of the device and are calibrated by means of steady-state tests.
- Dynamic parameters, which are responsible for making outputs vary over time and are calibrated through dynamic tests.
- Control logic parameters, which are responsible for switching between operation modes.

Both steady and dynamic parameters, as well as control logic parameters, are those summarized in Table 3.

Table 3 – Main parameters of the performance map, heat transfer coefficients and dynamic coefficients of the micro-CHP boiler.

Dependent variable		**Parameters**					
		Coefficients			Reference values		
Parameters of the performance map	$\dot{Q}^{se}_{net,max}$	a^{se}_1		a^{se}_2	$\dot{Q}^{se}_{net,ref}$	$T^{ref,se}_{cw,i}$	$\dot{m}^{ref,se}_{cw}$
	$\dot{E}^{se}_{net}$	b^{se}_1	b^{se}_2	b^{se}_3	$\dot{E}^{se}_{net,ref}$	T^{ref}_{head} $T^{ref,se}_{cw,i}$	$\dot{m}^{ref,se}_{cw}$
	η^{se}_{comb}	c^{se}_1		c^{se}_2	$\eta^{se}_{comb,ref}$	$T^{ref,se}_{cw,i}$	$\dot{m}^{ref,se}_{cw}$
	$\eta^{se}_{e,nom}$	d^{se}_1		d^{se}_2	$\eta^{se}_{e,ref}$	$T^{ref,se}_{cw,i}$	$\dot{m}^{ref,se}_{cw}$
	α^{se}_f		e^{se}			-	
	$\dot{Q}^{ab}_{net,max}$	a^{ab}_1		a^{ab}_2	$\dot{Q}^{ab}_{net,ref}$	$T^{ref,ab}_{cw,i}$	$\dot{m}^{ref,ab}_{cw}$
	η^{ab}_{comb}	c^{ab}_1		c^{ab}_2	$\eta^{ab}_{comb,ref}$	$T^{ref,ab}_{cw,i}$	$\dot{m}^{ref,ab}_{cw}$
	$\eta^{ab}_{t,nom}$	d^{ab}_1		d^{ab}_2	$\eta^{ab}_{t,ref}$	$T^{ref,ab}_{cw,i}$	$\dot{m}^{ref,ab}_{cw}$
	α^{ab}_f		e^{ab}			-	
Heat transfer coefficients	$\dot{Q}_{eng}$	$[UA]_{eng,1}$		$[UA]_{eng,2}$		$[UA]_{eng,3}$	
	$\dot{Q}_{HX}$	$[UA]_{HX}$		$[UA]_{HX,shutdown}$		$[UA]_{HX,standby}$	
	$\dot{Q}^{se}_{loss}$	$[UA]^{se}_{loss}$		$[UA]^{se}_{loss,shutdwon}$		$[UA]^{se}_{loss,standby}$	
	$\dot{Q}^{ab}_{loss}$	$[UA]^{ab}_{loss}$				$[UA]^{ab}_{loss,shutdown}$	
Dynamic parameters	-			$[MC]_{head}$			
	-			$[MC]_{eng}$			
	-			$[MC]_{HX}$			
	-			$[MC]_{ab}$			
	-			$T_{eng,nom}$			
	$\dot{E}^{se}_{net,warmup}$			$k_{e,1}$			
	$\dot{E}^{se}_{net,shutdown}$			$k_{e,2}$			
	$\dot{m}^{se}_{f,warmup}$	$k_{f,1}$		$k_{f,2}$		$k_{f,3}$	
Control logic parameters		T^{e}_{start}	$T^{start}_{head,nom}$	$T_{head,min}$	T^{e}_{stop}		T^{t}_{stop}

4.1.1. Steady operation

For a full characterization of the Stirling engine device, tests were run at full load as well as at part load. The steady-state experimental set comprises tests in function of both cooling water inlet temperature –from 30 ºC to 70 ºC– and volumetric flow –510 l/h, 670 l/h and 760 l/h–, as well as the generation set-point temperature, so that their influence on the energy performance can be determined. Further details of the results of these tests can be found at [37].

It was considered that the unit was operating under steady-state conditions provided that two conditions, evaluated on a 10-second basis, were met during at least 10 consecutive minutes:

- the cooling water return temperature variation with respect to the inlet set-point was lower than ±0.5 °C.
- the maximum deviation of the electric power with respect to the mean value of the measured interval was lower than 2%.

According to the results, the three main energy flows, i.e., fuel input and electrical and thermal outputs, are strongly dependent on the cooling water return temperature, while the cooling water flow has a lower influence.

First, concerning the thermal output and following a linear correlation, the lower the return temperature is, the higher the thermal production will be. This is mainly due to condensation gains since, once the return temperature has come below the dew-point temperature (around 50°C for natural gas), a higher part of the latent heat content of the exhaust gases is recovered when condensing their water vapour content. This increases even more as the circulating water flow grows.

The net thermal power output at full load presents a linear trend between 30 ºC and 60 ºC, which mainly comes from variations in the cooling water inlet temperature. Taking into consideration experimental data obtained in laboratory tests, the regression equation (Equation 13) was adjusted accordingly.

When analysing the effect of the cooling water return temperature on the electricity production, it can be observed that, as the engine works with higher cooling water temperatures, the electric output suffers substantial reductions. These variations, as reported in the model definition, have a clear linear trend. Meanwhile, the net electrical output of the engine is weakly dependent on the volumetric flow of the cooling water.

On the other hand, the engine energy input is regulated in order to maintain the temperature of the hot source within a range between 400 °C and 520 °C. This regulation is performed through the adjustment of the thermal power produced to that demanded. Furthermore, it can be appreciated that, for cooling water temperatures above 64 °C, the full-load operation changes its normal tendency, since an overheating

protection control starts to act and the temperature of the head of the engine is reduced as a consequence of reducing the energy input, thus working, in a certain manner, at part-load.

As previously mentioned, the engine is regulated in order to maintain a pre-fixed temperature value at the hot side of the engine and, in consequence, an apparent electric power. This regulation is achieved by varying the air mass flow introduced through the fan and, consequently, the fuel mass flow. Nevertheless, due to the fact that the LHV of the tests did not show large variations in the daily value, fuel variations remained bounded. In this sense, attending to the fuel input, its consumption on a volumetric basis, brought to normal conditions, presented very low variations. When the engine works at full load, once the air flow has been fixed, the gas valve remains open completely; consequently, in normal conditions where pressure and temperature conditions are fixed, the volumetric input must also remain virtually constant. Something similar happens when the analysis is tackled in terms of power.

The values of the main coefficients for the regression equations defined in the model, according to the experimental procedure hereby presented, are summarized in Table 4. When analysing the quality of the regression, two different statistical indicators were used: the adjusted R-squared (Adj-R^2) and the probability, also called p-value.

Table 4 – Summary of steady-state calibration coefficients of the SE.

Dependent variable	Coefficient	Value	Adj-R^2	p-value
$\dot{Q}_{net,max}^{se}$	a_1^{se}	-26.817	0.89	7.199E-10
α_t^{se}	a_3^{se}	113.077E-4	0.88	4.403E-10
$\dot{E}_{net}^{se}$	b_1^{se}	3.071	0.98	4.419E-51
	b_2^{se}	-2.189		1.221E-19
η_{comb}^{se}	c_1^{se}	-16.089E-5	0.91	1.257E-24
	c_2^{se}	82.214E-4		0.048
$\eta_{e,nom}^{se}$	d_1^{se}	58.526E-5	0.81	2.022E-06
α_f^{se}	e^{se}	1.118	0.98	5.418E-69

4.1.2. Transient operation

Concerning dynamic phases, an advanced procedure for identifying the main parameters of the model is required for calibrating the model. The parameter calibration method used allows all the MC and UA values to be calibrated at the same time, as well as the sensibility factors for electricity and fuel during transient processes. This process requires programming and implementing the model into the TRNSYS simulation environment and, once put together with an optimization tool such as GenOpt (Generic Optimization Program), an iterative process is carried out.

The calibration process, as represented in Figure 5, consists of an iterative calling between GenOpt, which reads and writes input/output text files, and TRNSYS. Once the optimization process is started, GenOpt initializes the variables to be calibrated –$\dot{F}_{se}$, T_{head}, $T^{se}_{cw,o}$ and $\dot{E}_{net}$– and provides this information to TRNSYS where, once the model is run and the output values are obtained, the cost function is calculated from simulated and real values. This cost function value is then transmitted to GenOpt to adjust the values of the parameters, between user-specified limits, and thus achieve the lowest possible cost function value. A cost function is a measure of how bad a model is in terms of its ability to estimate the relationship between independent and dependent variables.

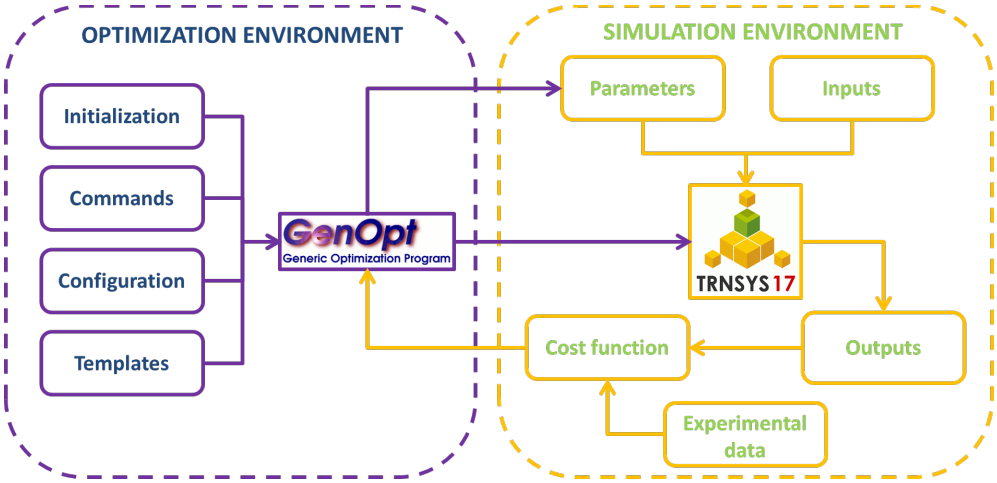

Figure 5 – Linking diagram between GenOpt and TRNSYS (adapted from Fernández et al. [40]).

In order to obtain the best result, apart from an adequate optimization function, an appropriate optimization algorithm should be chosen. In this sense, the calibration process was divided into two steps.

Firstly, as an approximation phase, the GPS Hooke-Jeeves algorithm was used to obtain acceptable results with a relatively low computational cost. This algorithm, as explained by Fernández et al. [40], is a hybrid algorithm for global optimization that combines restrictions set by the algorithm developed by Hooke and Jeeves with a global optimization pattern search (GPS).

Additionally, since GenOpt allows customized minimization algorithms that are not included by default to be added, a genetic algorithm was implemented to complete the second phase of the optimization. In this case, the Java Genetic Algorithms Package (JGAP) 3.6.2 was used. This package incorporates a robust and mature single-objective simple genetic algorithm which has been used for optimizing thermal systems [41-43].

Thus, in the second optimization step, the results obtained with the Hooke-Jeeves method were used to narrow the range of values and the optimization process was improved, while also avoiding local optimums.

This calibration process was applied to an experimental test where the volumetric flow and temperature of the returning cooling water were 700 l/h and 40 °C, respectively.

4.1.3. Calibration results

Results for the parameters identified through the calibration process are summarized in Table 5. It should be remarked that the effective heat transfer coefficients do not take into consideration the physical nature of the heat transfer processes, but aim to determine the combination of values that make the results of the model fit best with the reality. In order to physically approximate these processes, more detailed information should be obtained from the laboratory tests.

Table 5 – Calibration values for thermal masses, global heat transfer coefficients and sensitivity coefficients.

Parameter	Calibrated values	Units
$[UA]_{eng,normal}(W/K)$	19.650	W/K
$[UA]_{eng,shutdown}(W/K)$	11.435	W/K
$[UA]_{eng,standby}(W/K)$	0.5925	W/K
$[UA]_{HX,normal}(W/K)$	31.470	W/K
$[UA]_{HX,shutdown}(W/K)$	47.343	W/K
$[UA]_{HX,standby}(W/K)$	19.950	W/K
$[UA]_{loss,normal}(W/K)$	11.538	W/K
$[UA]_{loss,shutdown}(W/K)$	44.981	W/K
$[UA]_{loss,standby}(W/K)$	3.025	W/K
$[MC]_{head}$ (J/K)	1026.25	J/K
$[MC]_{eng}$ (J/K)	6741.25	J/K
$[MC]_{HX}$ (J/K)	20826	J/K
$k_{f,1}$	0.327	-
$k_{f,2}$	-10.529E-6	-
$k_{f,3}$	0.3	-
$k_{e,1}$	9.16E-3	-
$k_{e,2}$	2.580	-
$T_{eng,nom}$	206.9	°C

The cost function selected for the calibration process is the coefficient of variation of the root mean square error, CV(RMSE), calculated as follows:

$$CV(RMSE) = \frac{\sqrt{\frac{1}{n} \cdot \sum_{i=1}^{n} (\hat{y}_i - y_i)^2}}{\overline{y}}$$ Equation 50

where n is the number of measurement points of the sample; $\hat{y}_i$ stands for the predicted values –simulated temperatures and energy exchanges in the current case–; y_i stands for the actual values of the variables; and $\overline{y}$ is the mean value of the observed data.

Additionally, in order to complement the CV(RMSE), a statistical index which allows the error committed during a complete test to be quantified was also used, in terms of normalized mean bias error (NMBE):

$$NMBE(\%) = \frac{\sum_{i=1}^{n}(\hat{y}_i - y_i)}{\sum_{i=1}^{n}(\hat{y}_i)} \cdot 100 \qquad \text{Equation 51}$$

Table 6 – NMBE and CV(RMSE) for the full test calibration.

Variable	NMBE	CVRMSE
Fuel Power	-0.27%	5.54%
Net Electric Power	-0.22%	3.11%
Thermal Power	-1.18%	7.58%
Overall	0.56%	5.41%

The total computational cost of the calibration process –which is strongly dependent on the computer used– reached 70 minutes, where 37 minutes corresponded to the Hooke and Jeeves approximation phase, and the remaining 33 minutes were associated to the refinement phase carried out with the Genetic Algorithm.

This GenOpt-based calibration provides the best results achievable. Both in the dynamic phases, as well as in a full-test analysis, as summarized in Table 6, it can be seen that the statistical results are reasonably good. It must be pointed out that the mismatch existing in both warm-up and shut-down periods is mainly due to the stochastic nature of these transient processes. Thus, the description of the phenomena occurring during these periods is hardly improvable, taking into consideration the level of detail of the modelling approach used.

4.2.Parameter identification of the auxiliary burner

As far as the auxiliary burner is concerned, as done for the SE, different cooling water return temperature – 30 ºC to 60 ºC– and volumetric flow levels –500 l/h, 635 l/h and 725 l/h– were evaluated.

The results collected within the laboratory tests showed that the nominal thermal power oscillates significantly as a function of the return water temperature. This is mostly due to the latent heat recovery from the exhaust gases, since no significant impact of the water flow rate was detected. Additionally, these full-load tests evince that, when the thermal energy put into play is elevated, the higher the cold water flow is, the higher the thermal recovery will be. Meanwhile, if the part-load operation is to be attended, no appreciable difference in the aforementioned sense is detected when the auxiliary burners work at the

minimum load. The minimum part-load ratio achievable, independently of the cooling water temperature or mass flow imposed, is 0.3.

As summarized in Table 7, all the steady-state calibration values show good statistical indicators.

Table 7 – Summary of steady-state calibration coefficients of the AB.

Dependent variable	Coefficient	Value	Adj-R^2	p-value
$\dot{Q}^{se}_{net,max}$	a_1^{ab}	-97.770	0.88	5.131E-11
	a_2^{ab}	8601.963		1.723E-02
η^{ab}_{comb}	b_1^{ab}	-2.372E-03	0.94	1.365E-20
$\eta^{ab}_{t,nom}$	c_1^{ab}	-3.865E-03	0.89	2.531E-11
	c_2^{ab}	3.624E-01		9.021E-03
α_f^{ab}	d^{ab}	1.03	0.99	1.716E-35

Taking into account that, as concluded for the Stirling engine dynamic parameter identification, GenOpt based calibration provides the best results, the auxiliary burner was accordingly calibrated. In this case, due to the low number of dynamic parameters to identify ($[MC]_{ab}$and $[UA]^{ab}_{loss}$), the calibration was immediately carried out using the genetic algorithm.

5. MODEL VALIDATION

In this section, the previously defined and calibrated model is validated by means of a comparison with different experimental data sets. Additionally, it is compared with the model proposed by Kelly and Beausoleil-Morrison [18] within the Annex 42 framework. The steady-state validation presented in section 5.1 is carried out from different data-sets that emerge from the combination of different return mass flows and temperatures of the cooling water. Additionally, the dynamic validation and the part-load validation were carried out taking into consideration two tests with different constraints to those of the test used for calibrating the model.

In this sense, whereas the calibration was carried out with a test of 700 l/h and 40 °C of respective volumetric flow and return temperature of the cooling water, two other tests were used for the validation:

- Test A: Full test with 490 l/h and 40 °C (6-hours length, see section 5.2)
- Test B: Full test with 540 l/h and 50 °C, including part-load operation (9-hours length, see section 5.3)

All these tests were conducted in the experimental facility described in section 3 and depicted in Figure 6.

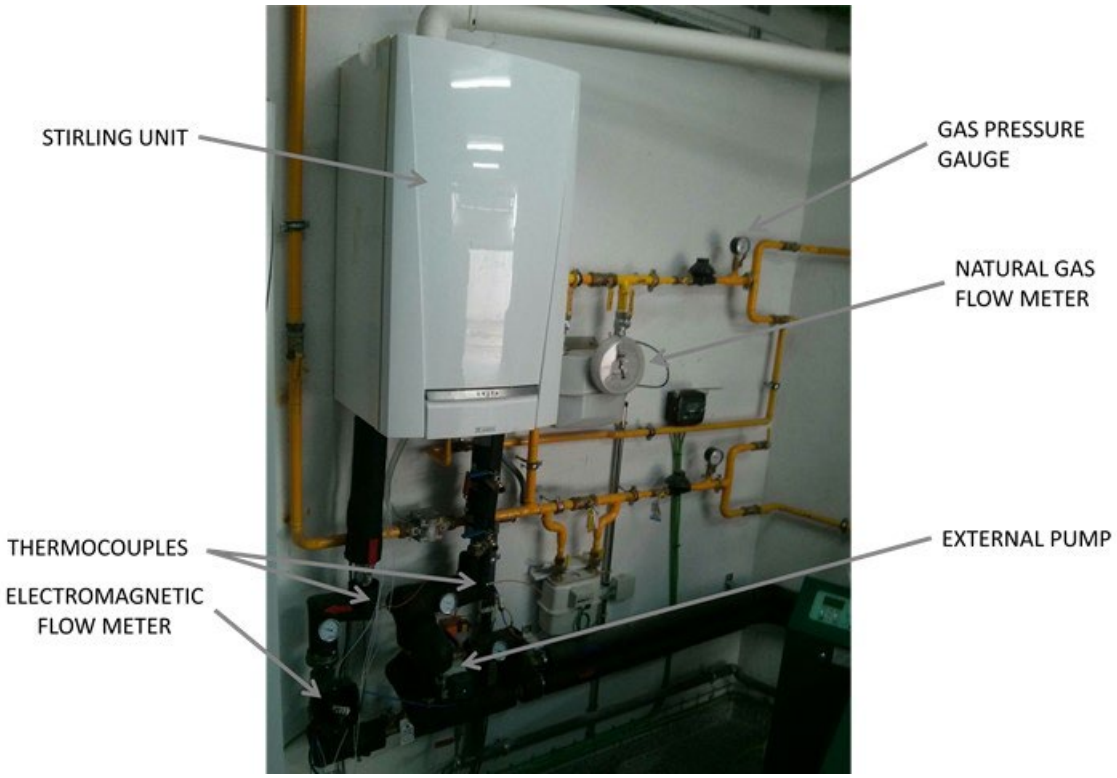

Figure 6 – Picture of the Stirling engine test rig.

5.1.Steady-state validation

The comparison between the actual experimental values and the two main outputs provided by the model under steady-state conditions are summarized in Table 8, for two different mass flow levels and 5 temperature levels.

Table 8 – Steady-state validation results for the SE: comparison with experimental results.

	$T_{cw,i}$ level	$\dot{E}_{net}$			$T^{se}_{cw,o}$		
	(°C)	Measured (W)	Predicted (W)	NMBE (%)	Measured (°C)	Predicted (°C)	NMBE (%)
635 l/h	30	964	955	-0.93	37.09	36.88	-0.57
	40	944	945	0.11	46.46	46.28	-0.39
	50	905	923	1.99	55.97	56.10	0.23
	60	892	901	1.01	65.71	65.79	0.12
	70	761	779	2.36	75.31	75.55	0.32
765 l/h	30	961	961	-0.02	36.49	36.39	-0.27
	40	943	944	0.01	45.77	45.37	-0.87
	50	938	923	-1.60	55.28	55.09	-0.34
	60	906	902	-0.44	64.96	65.02	0.09
	70	798	814	2.00	72.61	72.60	-0.01

Meanwhile, results for two tests with lower cooling water mass flows are graphically shown, in terms of power, in the subsequent figures, when the dynamics of the model are analysed (Test A and Test B). The results confirm, by comparing outputs in terms of power and on an NMBE basis, that the model is able to faithfully reproduce the steady-state performance of the micro-CHP unit. The main discrepancy found in this comparison lies in the electricity output. This difference may respond, in part, to the suitability of the correlations used to model the performance map of the engine, but also to the uncertainty of the measurement of the gross electric power provided by the engine.

5.2.Dynamic validation (Test A)

The dynamic validation of the model was carried out taking into consideration Test A and, visually, when assessing the part-load validation, with Test B.

While the results corresponding to a complete on-off cycle, when operating at full load (Test A), are presented in Figure 7 to Figure 9; the comparison of the results corresponding to the warm-up and shutdown periods of the same test are presented from Figure 10 to Figure 12 and in Figure 13 and Figure 14, respectively.

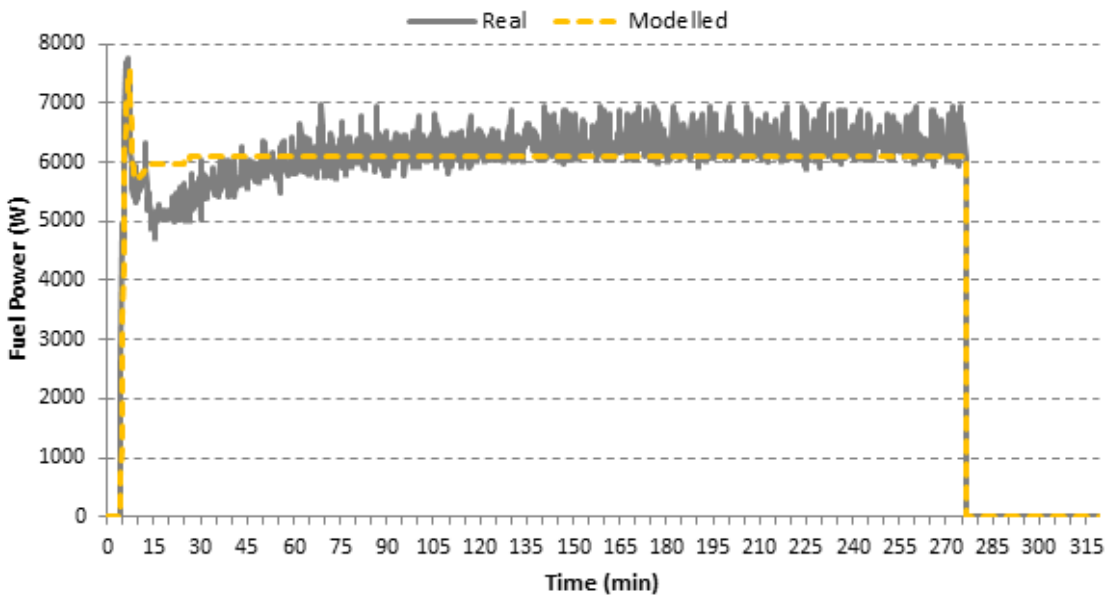

Figure 7 – Full-load validation test of the Stirling engine: fuel power (Test A).

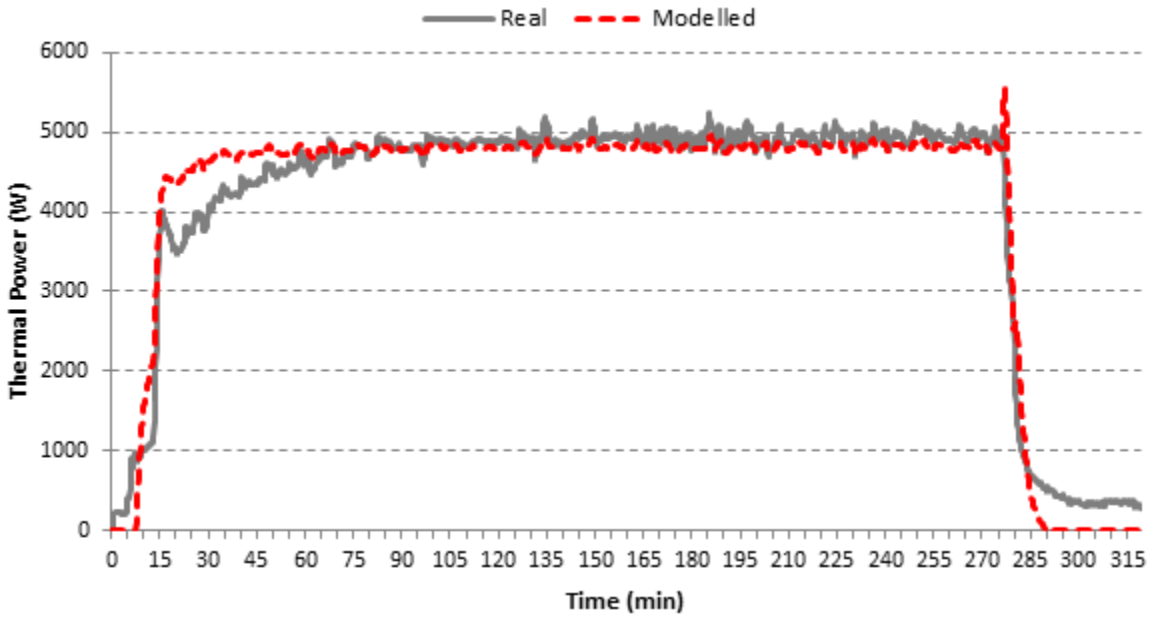

Figure 8 – Full-load validation test of the Stirling engine: thermal power (Test A).

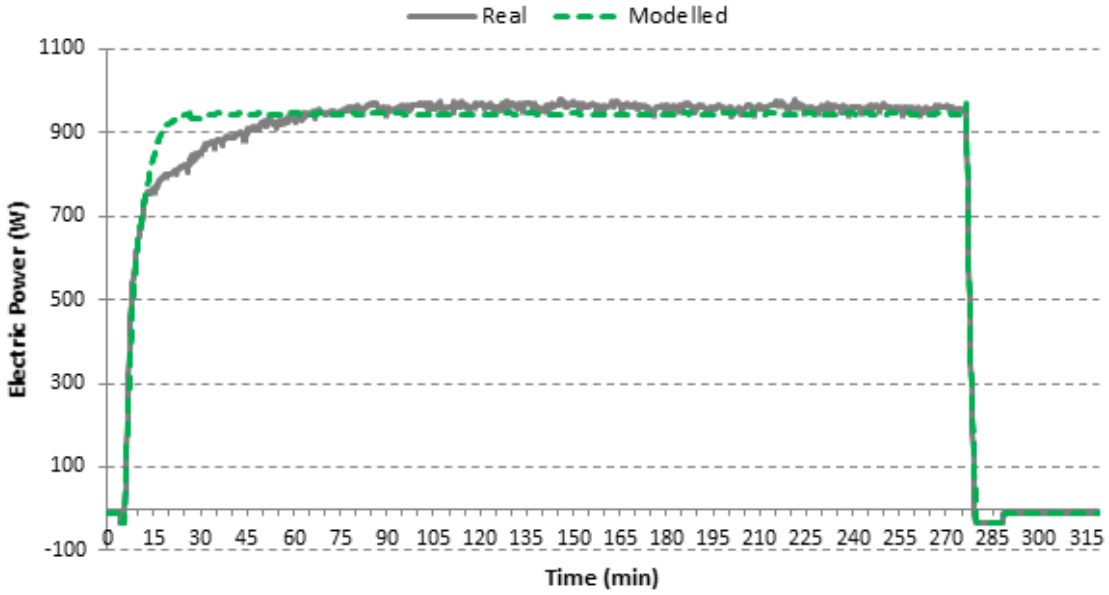

Figure 9 – Full-load validation test of the Stirling engine: electric power (Test A).

Additionally, the dynamic phases of Test A were separately analysed, complementing the analysis by a comparison with the model developed in the Annex 42, which was calibrated following the calibration protocol therein presented [44] and the same experimental data set used for calibrating the model developed in this paper.

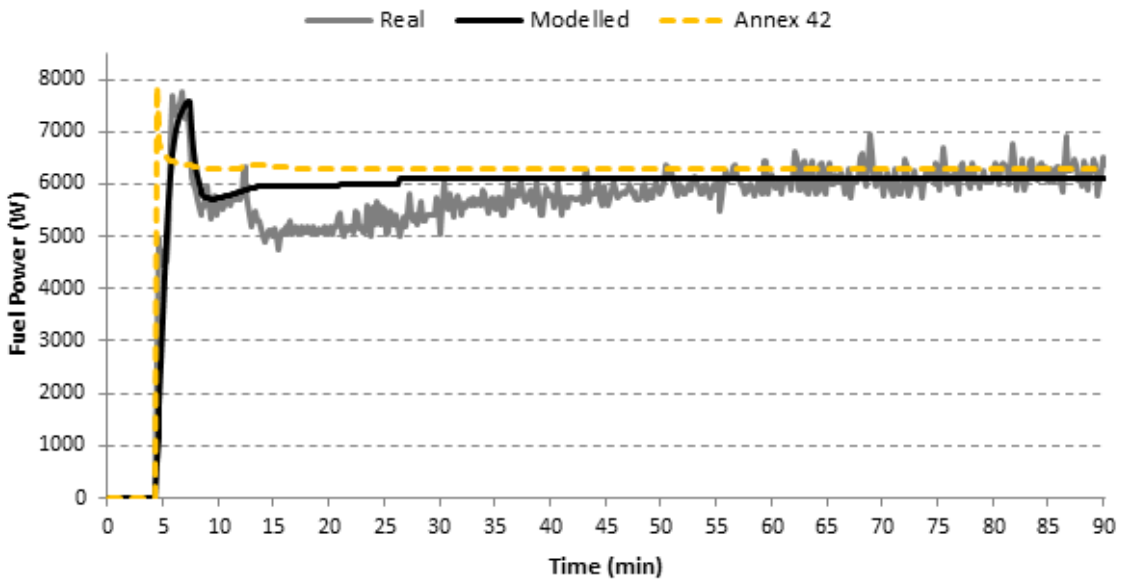

Figure 10 – Real and simulated fuel power during the warm-up period (Test A).

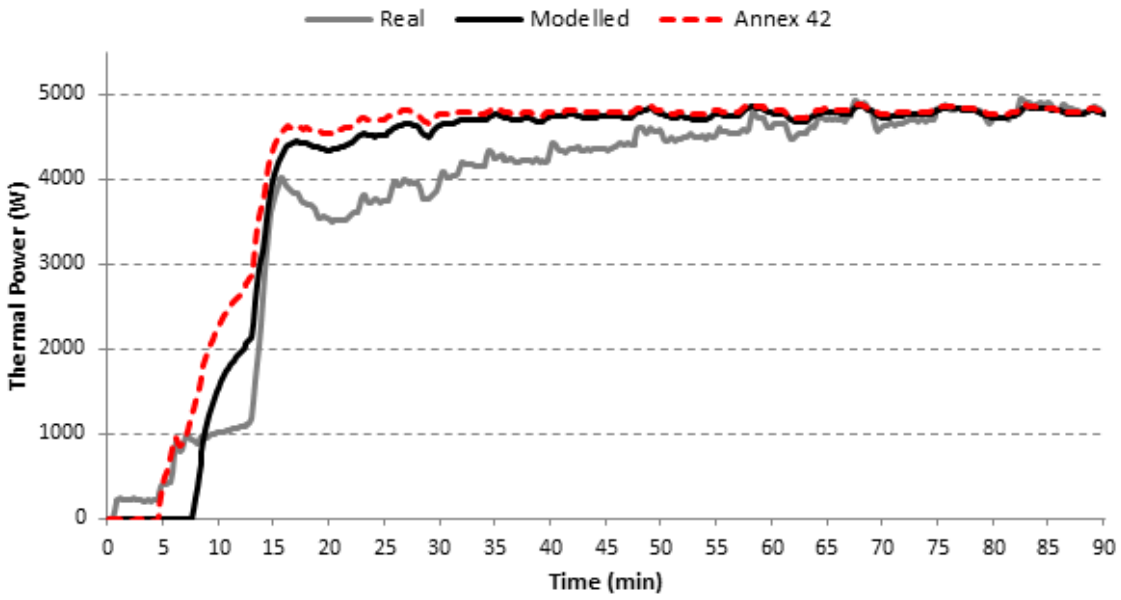

Figure 11 – Real and simulated thermal power during the warm-up period (Test A).

As observed, the model has good agreement with the model developed within the Annex 42 context, as well as with the experimental data in both dynamic phases.

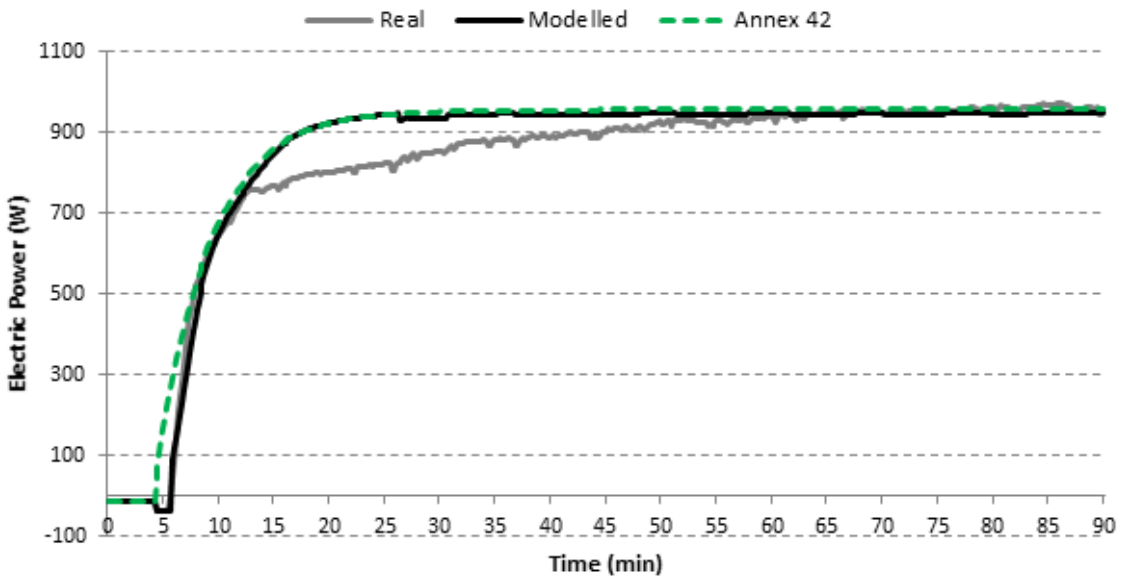

Figure 12 – Real and simulated electric power during the warm-up period (Test A).

In the case of the warm-up period, whose results are depicted from Figure 10 to Figure 12, the main discrepancy, as previously commented in section 4.1.3, resides in the second part of the fuel power during this phase. The internal control makes the fuel power drop in two steps from the peak achieved during the overshoot that takes place when the engine switches on before it tends to the nominal value in steady-state conditions. Since the natural gas counter sends out a very frequent pulse (every 10 dm^3 while traditional residential gas counters generate a pulse every 100 dm^3), this effect is accurately measured, but the model is not able to reproduce such control in all its extension, and only takes into consideration the first decline.

It is this fuel overfeed considered by the model that takes both thermal and electric outputs to slightly above the measured values. However, provided that the micro-CHP unit operates over long periods, this fact will not have a significant impact in the final results. Additionally, if the model is to be used with time-steps greater than the 10-second frequency considered during the calibration and validation of the model in this paper, as typically done in building energy simulation applications, this difference is drastically reduced.

Even so, the NMBE of the three energy exchanges are 3.6%, 6.8% and 3.6%, respectively, for the fuel input, and the heat and electricity outputs.

Concerning the comparison with the results achieved with the already validated model of the Annex 42, it can be observed that the fuel overshoot of the current model adapts better to reality, while the energy outputs are very similar for both models. In the case of the electricity output, however, it can be seen that, whilst the model developed within this article fits the initialization of the power output, the Annex 42 comes to this starting point ahead of time.

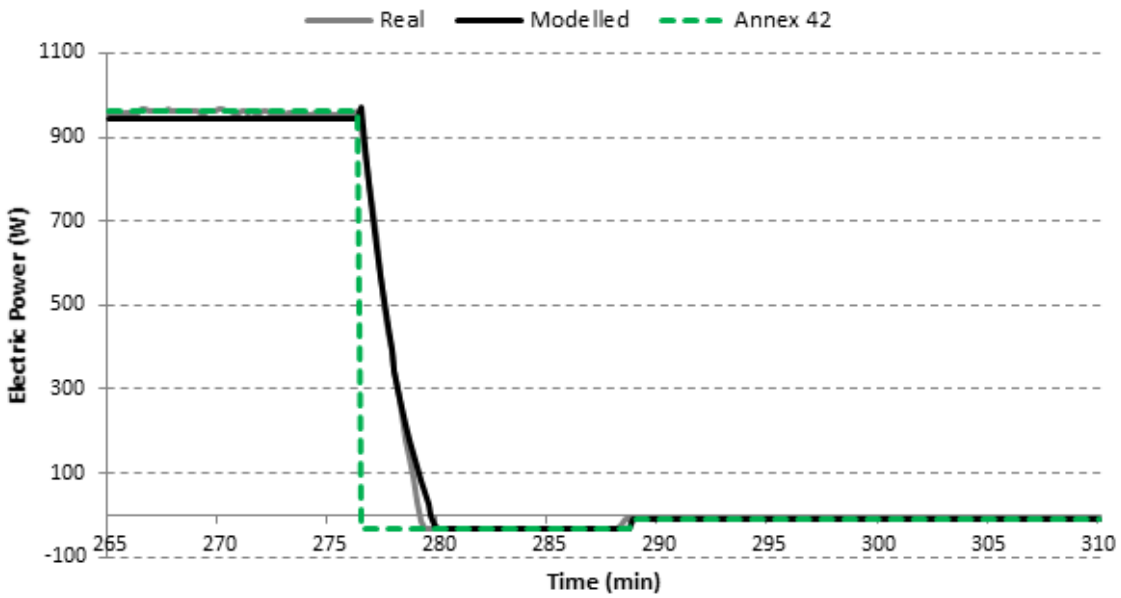

Figure 13 – Real and simulated electric power during shutdown and standby periods.

In the case of the shut-down period, while the electric output is almost identical (Figure 13), the model is also capable of following the tendency of the thermal output during the shut-down process (Figure 14). Meanwhile, the discrepancy existing during the stand-by phase, which is partially due to the offset existing in the data acquisition, is negligible when the engine is integrated within a thermal installation. This latter aspect responds to the fact that, once the temperature of the head of the engine falls below 130 °C, the pump will stop together with the air intake fan; consequently, the thermal power output will be zero.

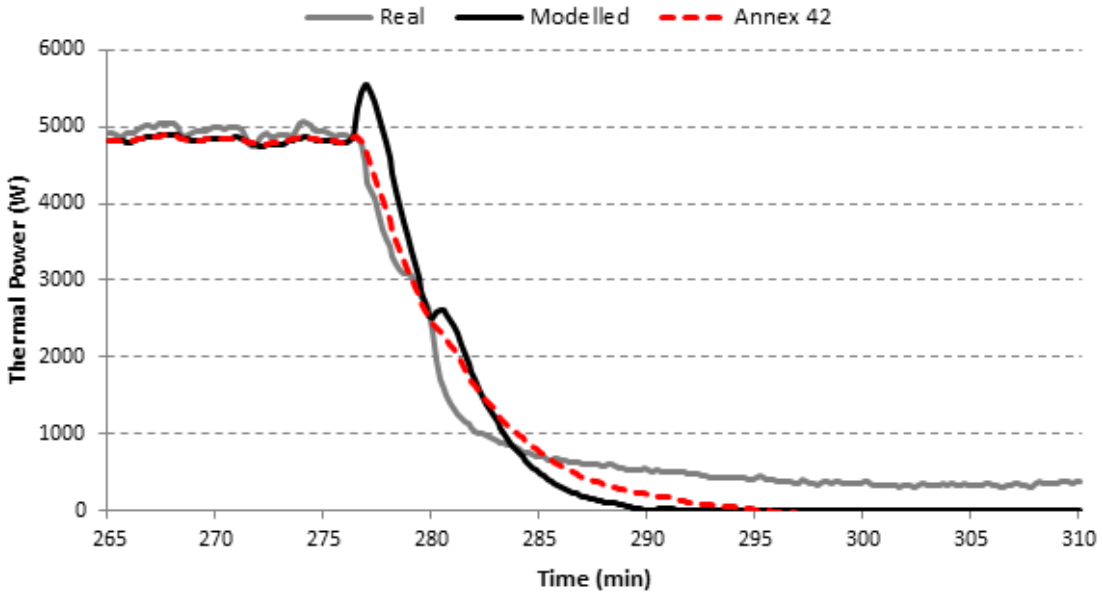

Figure 14 – Real and simulated thermal power during shutdown and standby periods (Test A).

In both output cases, the NMBE is below 10% during this mode of operation, which difference constitutes 0.1% of the energy produced during the whole test in the case of the thermal output, while in the case of the electric production, it is virtually zero.

Attending to the Annex 42 model, it was checked that the thermal output difference between both models is only 1.6% (6.3 Wh). Meanwhile, the electric output modelled, contrary to the Annex 42 model, does not overlook the production that takes place once the fuel flow is cut off.

The main results of the two models compared, with respect to the real data, are summarized in Table 9, where it can be appreciated that both models can predict the performance of the engine with a low error and, additionally, both models fit each other with high precision.

Table 9 – Comparison of the results of the experimental test, the proposed model and the Annex 42 model (Test A).

	Measurements (kWh)			NMBE (%)	
	Experimental	Model	Annex 42 model	Model	Annex 42 model
Fuel input	27.98	27.59	28.60	-1.4	2.2
Thermal output	21.39	21.48	21.72	0.4	1.5
Electric output	4.22	4.22	4.27	-0.1	1.1

5.3.Part-load validation (Test B)

As far as part-load performance is concerned, as depicted in Figure 15 for Test B, very good agreement between experimental and modelled data is reached, whatever the turndown ratio is.

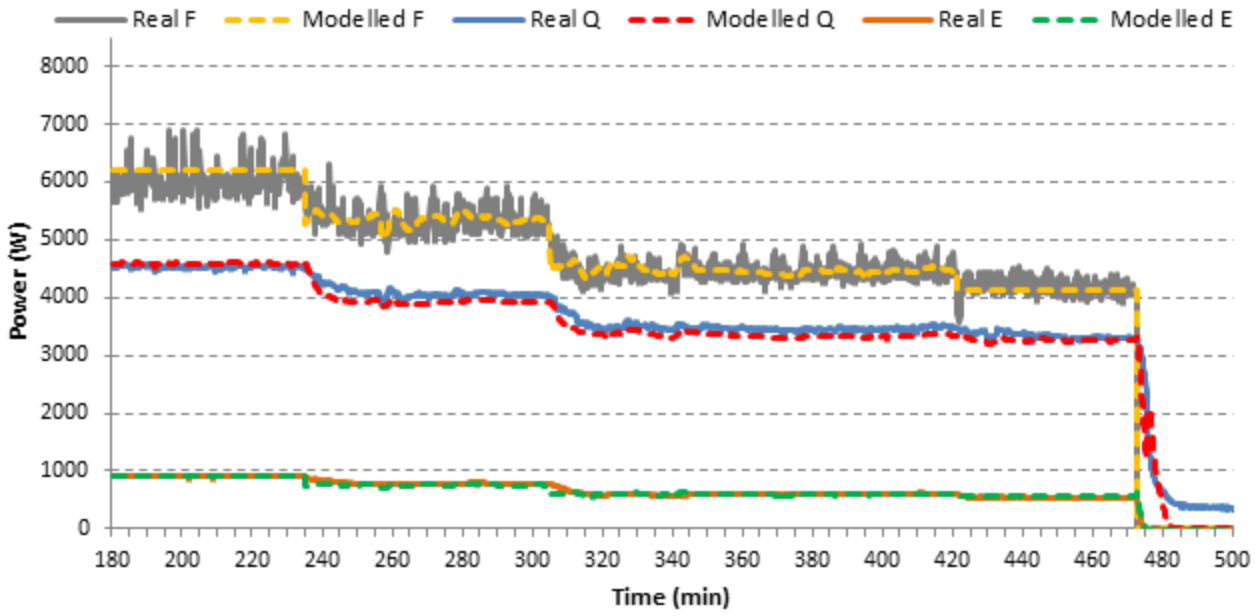

Figure 15 – Real and simulated power exchanges during part-load operation (Test B).

In this sense, nevertheless, it can be appreciated that the thermal output predicted by the model at part-load is slightly below the real value. This is due to the fact that the test was carried out with a fixed cooling water temperature at the inlet; while, in order to modulate the engine, it was the set-point temperature that was variable. Since the engine is controlled in order to reach the set-point temperature measured by its internal sensor, differences between the internal and external measurements make the set-point temperature not be exactly the same as that imposed. Accordingly, the fuel power can also differ slightly before the engine switches off, due to this discrepancy in the set-point temperature and to low errors when predicting the temperature of the head of the engine.

On the other hand, it can also be appreciated that the shutdown process, as happened for the full-load validation test, is successfully modelled, for both thermal and electric outputs.

Finally, concerning the auxiliary burner, the power-based results, summarized in Table 10, prove that the model proposed successfully fulfils its objective.

Table 10 – Validation results for the auxiliary burner.

		Fuel input			Thermal output		
	$T_{cw,i}$ level	Measured (W)	Calculated (W)	NMBE (%)	Measured (W)	Calculated (W)	NMBE (%)
635 l/h	30	19463	20094	3.24	17156	17910	4.39
	35	19676	19990	1.60	17260	17599	1.96
	40	19407	19851	2.29	16543	16829	1.73
	50	19738	19587	-0.77	16063	15873	-1.18
720 l/h	30	20618	20124	-2.40	18091	18442	1.94
	35	19740	20027	1.45	17296	17869	3.31
	40	20231	19888	-1.70	17100	17105	0.03
	50	20069	19630	-2.19	15930	15761	-1.06

6. CONCLUSIONS

This paper deals with the modelling, experimental characterization and validation of Stirling engine-based residential micro-CHP units. A new modelling approach is presented in this work with the objective of relieving the deficiencies associated to previous models, as well as strengthening their strong points.

The developed model, due to its architecture and topology, is generic and adaptable to most of the Stirling engine-based micro-CHP units available in the market. Due to its scope of application, it is conceived in terms of a grey-box modelling approach, which combines an analytical description of some of the physical phenomena together with empirical data. One of the main strengths of the model lies in the consideration of the part-load operation of this kind of devices, which is generally overlooked in research previously

presented by other authors. Additionally, other phenomena related to the main energy exchanges are better addressed and adapted to the architecture of this kind of devices.

Once the mathematical model is defined and implemented in a BES environment, the experimental characterization of a Stirling micro-CHP unit is addressed. For that purpose, an experimental test-rig was developed, where the engine was integrated. This test-rig, which is part of an ambitious experimental installation designed and developed within the context of this research, fulfils all the necessities derived from the modelling for its calibration and validation. Through the testing routine, which encompasses the evaluation of every operation mode the engine can operate at, it is verified that the main source of uncertainty when evaluating the different measurements lies in the fuel determination.

Subsequently, using the empirical data obtained, the model proposed is calibrated. This calibration process, due to its relative complexity, requires sophisticated parameter identification techniques based on optimization algorithms that allow the deviation with respect to real data to be minimized (0.56% overall error during a complete on-off cycle).

Finally, the model proposed is validated. For the case of the engine, even though predicted values can differ slightly from the actual values under some working conditions, the results present a good agreement in general terms, with errors below 2.4% and 0.9% in all cases for the net electric power and the cooling water outlet temperature, respectively. During the most critical transients, the NMBE of the three energy exchanges during a warming-up phase are 3.6%, 6.8% and 3.6%, respectively, for the fuel input and the heat and electricity outputs; while the NMBE for both outputs is below 10% during the shutting-down process. Finally, if a full-length test is examined, the mean errors for the energy exchanges due to fuel input, thermal output and electrical outputs were 1.4%, 0.4% and 0.1%, respectively.

Being a simplified model whose appliance is aimed at use in building energy simulation tools, the model can definitely be considered to represent the performance of the engine accurately, while also maintaining quite a simple structure in comparison with analytical and numerical approaches.

ACKNOWLEDGEMENTS

This work was supported by the Spanish Ministry of Science, Innovation and Universities and the European Regional Development Fund through the MONITHERM project ‘Investigation of monitoring techniques of occupied buildings for their thermal characterization and methodology to identify their key performance indicators’, project reference RTI2018-096296-B-C22 (MCIU/AEI/FEDER, UE); and by the European Union’s Interreg Sudoe Programme through the ARCAS project ‘New assessment Methodology for social, sustainable and eco-friendly housing. Climate architecture for the Sudoe's area’, project reference SOE3/P3/E0922. The

authors would also like to specially thank the Laboratory for Quality Control in Buildings (LCCE) of the Basque Government, for its financial and technical means.

Additionally, Iker González-Pino acknowledges the financial support of the Basque Government, through the Department of Education, Universities and Research's Personnel Research Training Program (BFI-2011-153).

REFERENCES

[1] Eurostat, Statistics Database - Energy statistics - Supply, transformation, consumption (2012).

[2] European Commission, COMMUNICATION FROM THE COMMISSION TO THE EUROPEAN PARLIAMENT, THE COUNCIL, THE EUROPEAN ECONOMIC AND SOCIAL COMMITTEE AND THE COMMITTEE OF THE REGIONS A policy framework for climate and energy in the period from 2020 to 2030 (2014).

[3] European Commission, EU climate action. Climate strategies & targets: 2050 long-term strategy, https://ec.europa.eu/clima/policies/strategies/2050_en#tab-0-0 (2019).

[4] Official Journal of the European Union, DIRECTIVE 2012/27/UE of the European Parliament and of the Council of 25 October 2012 on the energy efficiency, amending Directives 2009/125/EC and 2010/30/EU and repealing Directives 2004/8/EC and 2006/32/EC (2012).

[5] Official Journal of the European Union, Directive (EU) 2018/844 of the European Parliament and of the Council of 30 May 2018 amending Directive 2010/31/EU on the energy performance of buildings and Directive 2012/27/EU on energy efficiency (2018).

[6] C. Roselli, M. Sasso, S. Sibilio, P. Tzscheutschler, Experimental analysis of microcogenerators based on different prime movers, Energy Build. 43 (2011) 796-804.

[7] S. Martinez, G. Michaux, P. Salagnac, J. Bouvier, Micro-combined heat and power systems (micro-CHP) based on renewable energy sources, Energy Conversion and Management 154 (2017) 262-285.

[8] A.C. Ferreira, J. Silva, S. Teixeira, J.C. Teixeira, S.A. Nebra, Assessment of the Stirling engine performance comparing two renewable energy sources: Solar energy and biomass, Renewable Energy 154 (2020) 581-597.

[9] D.G. Thombarse, Stirling Engine: Micro-CHP System for Residential Application, in: K.H.J. Buschow, R.W. Cahn, M.C. Flemings, B. Ilschner, E.J. Kramer, S. Mahajan, P. Veyssière (Eds.), Encyclopedia of Materials: Science and Technology (Second Edition), Elsevier, Oxford, 2008, pp. 1-8.

[10] K. Wang, S.R. Sanders, S. Dubey, F.H. Choo, F. Duan, Stirling cycle engines for recovering low and moderate temperature heat: A review, Renewable and Sustainable Energy Reviews 62 (2016) 89-108.

[11] H. Hachem, R. Gheith, F. Aloui, S. Ben Nasrallah, Technological challenges and optimization efforts of the Stirling machine: A review, Energy Conversion and Management 171 (2018) 1365-1387.

[12] I. González-Pino, A. Campos-Celador, E. Pérez-Iribarren, J. Terés-Zubiaga, J.M. Sala, Parametric study of the operational and economic feasibility of Stirling micro-cogeneration devices in Spain, Appl. Therm. Eng. 71 (2014) 821-829.

[13] I. González-Pino, E. Pérez-Iribarren, A. Campos-Celador, J. Las-Heras-Casas, J.M. Sala, Influence of the regulation framework on the feasibility of a Stirling engine-based residential micro-CHP installation, Energy 84 (2015) 575-588.

[14] I. González-Pino, E. Pérez-Iribarren, A. Campos-Celador, J. Terés-Zubiaga, Analysis of the integration of micro-cogeneration units in space heating and domestic hot water plants, Energy 200 (2020) 117584.

[15] G. Conroy, A. Duffy, L.M. Ayompe, Economic, energy and GHG emissions performance evaluation of a WhisperGen Mk IV Stirling engine μ-CHP unit in a domestic dwelling, Energy Conversion and Management 81 (2014) 465-474.

[16] M. Sheykhi, M. Chahartaghi, M.M. Balakheli, B.A. Kharkeshi, S.M. Miri, Energy, exergy, environmental, and economic modeling of combined cooling, heating and power system with Stirling engine and absorption chiller, Energy Conversion and Management 180 (2019) 183-195.

[17] M. Sheykhi, M. Chahartaghi, M.M. Balakheli, S.M. Hashemian, S.M. Miri, N. Rafiee, Performance investigation of a combined heat and power system with internal and external combustion engines, Energy Conversion and Management 185 (2019) 291-303.

[18] B. Kelly N. I., Specifications for modelling fuel cell and combustion-based residential cogeneration devices within whole-building simulation programs, IEA/ECBCS Annex 42 (2007).

[19] G. Dochat, SPDE/SPRE final summary report, SPDE/SPRE Final Summary Report 187086 (1993).

[20] J.B. Heywood, Internal Combustion Engine Fundamentals, McGraw-Hill, inc., New York, USA, 1998.

[21] I. Urieli, D. Berchowitz, Stirling cycle engine analysis, Adam Hilger Ltd., Bristol, UK, 1984.

[22] F. Cascella, M. Sorin, F. Formosa, A. Teyssedou, Modeling the dynamic and thermodynamic operation of Stirling engines by means of an equivalent electrical circuit, Energy Conversion and Management 150 (2017) 295-303.

[23] B. Rutczyk, I. Szczygieł, Z. Buliński, A zero-dimensional, real gas model of an α Stirling engine, Energy Conversion and Management 199 (2019) 111995.

[24] S. Zhu, G. Yu, J. O, T. Xu, Z. Wu, W. Dai, E. Luo, Modeling and experimental investigation of a free-piston Stirling engine-based micro-combined heat and power system, Appl. Energy 226 (2018) 522-533.

[25] G. Valenti, P. Silva, N. Fergnani, G. Di Marcoberardino, S. Campanari, E. Macchi, Experimental and Numerical Study of a Micro-cogeneration Stirling Engine for Residential Applications, Energy Procedia 45 (2014) 1235-1244.

[26] J.M. Pearce, B.A.T. Al Zahawi, D.W. Auckland, F. Starr, Electricity generation in the home: evaluation of single-house domestic combined heat and power, Science, Measurement and Technology, IEE Proceedings - 143 (1996) 345-350.

[27] J.M. Pearce, B.A.T. Al Zahawi, R. Shuttleworth, Electricity generation in the home: modelling of single-house domestic combined heat and power, Science, Measurement and Technology, IEE Proceedings - 148 (2001) 197-203.

[28] S. Thiers, B. Aoun, B. Peuportier, Experimental characterization, modeling and simulation of a wood pellet micro-combined heat and power unit used as a heat source for a residential building, Energy Build. 42 (2010) 896-903.

[29] G. Conroy, A. Duffy, L.M. Ayompe, Validated dynamic energy model for a Stirling engine μ-CHP unit using field trial data from a domestic dwelling, Energy Build. 62 (2013) 18-26.

[30] W. Uchman, J. Kotowicz, L. Remiorz, An Experimental Data-Driven Model of a Micro-Cogeneration Installation for Time-Domain Simulation and System Analysis, Energies 13 (2020) 2759.

[31] A. Cacabelos, P. Eguía, J.L. Míguez, G. Rey, M.E. Arce, Development of an improved dynamic model of a Stirling engine and a performance analysis of a cogeneration plant, Appl. Therm. Eng. 73 (2014) 608-621.

[32] C. Ulloa, J.L. Míguez, J. Porteiro, P. Eguía, A. Cacabelos, Development of a transient model of a stirling-based CHP system, Energies 6 (2013) 3115-3133.

[33] K. Lombardi, V.I. Ugursal, I. Beausoleil-Morrison, Proposed improvements to a model for characterizing the electrical and thermal energy performance of Stirling engine micro-cogeneration devices based upon experimental observations, Appl. Energy 87 (2010) 3271-3282.

[34] J.-. Bouvenot, B. Andlauer, P. Stabat, D. Marchio, B. Flament, B. Latour, M. Siroux, Gas Stirling engine μCHP boiler experimental data driven model for building energy simulation, Energy Build. 84 (2014) 117-131.

[35] EHE, Whispergen EU1, Efficient Home Energy S.L. 2012 (2008).

[36] Departamento de Medio Ambiente, Planificación Territorial y Vivienda, Laboratorio de Control de Calidad en la Edificación, Gobierno Vasco, http://www.euskadi.eus/lcce 2017 (2018).

[37] I. González-Pino, Modelling, experimental characterization and simulation of Stirling engine-based micro-cogeneration plants for residential buildings (2019).

[38] A. Bengoetxea, M. Fernandez, E. Perez-Iribarren, I. Gonzalez-Pino, J. Las-Heras-Casas, A. Erkoreka, Control strategy optimization of a Stirling based residential hybrid system through multi-objective optimization, Energy Conversion and Management 208 (2020) 112549.

[39] Bureau International des Poids et Mesures, Commission électrotechnique internationale, Organisation internationale de normalisation, Guide to the Expression of Uncertainty in Measurement, International Organization for Standardization, 1995.

[40] M. Fernández, P. Eguía, E. Granada, L. Febrero, Sensitivity analysis of a vertical geothermal heat exchanger dynamic simulation: Calibration and error determination, Geothermics 70 (2017) 249-259.

[41] V. Machairas, A. Tsangrassoulis, K. Axarli, Algorithms for optimization of building design: A review, Renewable and Sustainable Energy Reviews 31 (2014) 101-112.

[42] A. T. D. Perera, M. P. G. Sirimanna, A novel simulation based evolutionary algorithm to optimize building envelope for energy efficient buildings, 7th International Conference on Information and Automation for Sustainability (2014) 1-6.

[43] E. Pérez-Iribarren, Optimización en la operación y el diseño de plantas de microcogeneración para edificios de viviendas. (2016).

[44] I. Beausoleil-Morrison, Experimental investigation of residential cogeneration devices and calibration of Annex 42 Models, IEA/ECBCS Annex 42 (2007).